Sustainable Chemistry and Pharmacy 43 (2025) 101880

Contents lists available at ScienceDirect

Sustainable Chemistry and Pharmacy

journal homepage: www.elsevier.com/locate/scp

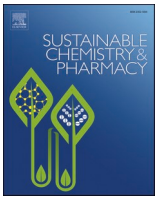

Valorization of PDMS-coated glassine wastepaper for microcrystalline cellulose: Extraction and physicochemical characterization

Nuhairi Alias [a], Che Rozid Mamat [a,*], Zaiton Abdul Majid [a], Nur Faraliana Japri [a], Nur Hafizah A. Khalid [b]

[a] Department of Chemistry, Faculty of Science, Universiti Teknologi Malaysia, 81310 Johor Bahru, Johor, Malaysia
[b] Centre for Advanced Composite Materials (CACM), Faculty of Civil Engineering, Universiti Teknologi Malaysia, 81310 Johor Bahru, Johor, Malaysia

ARTICLE INFO

Keywords:
Microcrystalline cellulose
Valorization
Wastepaper
PDMS
Glassine

ABSTRACT

Polydimethylsiloxane (PDMS)-coated glassine wastepaper present challenges to waste management, particularly due to its limited recyclability and the presence of polymer coating. The high cellulose and minimal lignin content in PDMS-coated glassine wastepaper makes it a good candidate for microcrystalline cellulose (MCC) extraction. A 5% sodium hydroxide (NaOH) and sodium hypochlorite (NaOCl) were used to extract MCC from the PDMS-coated glassine wastepaper. Sodium hypochlorite (NaOCl) ranging from 1.0 to 3.0% was applied to assess its influence on the physicochemical properties of extracted MCC and subsequently compared to the commercial MCC. The samples were characterized by Fourier transform infrared spectroscopy (FTIR), X-ray diffraction (XRD), thermogravimetric analysis (TGA), particle size analysis (PSA) and transmission electron microscopy (TEM). The study revealed that the properties of extracted MCC closely resemble to those of commercial MCC with 5% NaOH and 1.6% NaOCl achieving the highest crystallinity index (CrI) of 78.90%, the lowest *d*-spacing of 3.91 Å and activation energy of 25.349 $kJmol^{-1}$. The crystallinity showed a decline with increasing NaOCl concentration beyond 1.6% due to intensified oxidative bleaching. The study has also shown that the extraction of MCC from PDMS-coated glassine wastepaper was possible without the use of acid hydrolysis.

1. Introduction

Waste is generally classified into two main categories: municipal solid waste, which includes waste produced by households and small businesses, and non-municipal waste, which encompasses waste generated by industrial activities, as reported by the United Nation Environment Programme (Lenkiewicz *et* al., 2024). The importance of managing industrial waste efficiently was highlighted by Khoshsepehr and co-workers (2023), who emphasized the need for the industrial sectors to adopt smart technologies for better waste management. According to Kaza et al. (2018) in the World Bank publication "A Global Snapshot of Solid Waste Management to 2050", paper products accounted 17% of the global waste composition. Furthermore, the United Nations Office on Drugs and Crime reported

* Corresponding author.
E-mail addresses: nuhairi3@graduate.utm.my (N. Alias), cherozid@utm.my (C.R. Mamat), zaitonmajid@utm.my (Z.A. Majid), nfaraliana2@graduate.utm.my (N.F. Japri), nur_hafizah@utm.my (N.H.A. Khalid).

https://doi.org/10.1016/j.scp.2024.101880
Received 26 September 2024; Received in revised form 13 November 2024; Accepted 30 November 2024

in "Unwaste Trendspotting Alert," (2023) that paper waste and its industrial by-products are often disposed in landfills or released into the environment. The rising awareness of environmental concerns due to huge amount of waste generated during production have forced the industries to find alternative ways in utilizing the waste that were normally burned or disposed in the landfills. To be the second most disposed material among others, paper is made up of fibrous cellulose as the major component which is build up from polysaccharide structure with numerous hydroxyl groups, that makes paper hydrophilic in nature. To improve the properties of paper such as water repellence, chemical stability and adhesion, some paper products have been treated with polymer coatings such as polydimethylsiloxane (PDMS) (Fu et al., 2022; Söz, 2022), polyethylene (Žgajnar Gotvajn and Kalčíková, 2018), poly(ethylene terephthalate) (Lei et al., 2018), resin (Iwamiya et al., 2022), polyvinyl alcohol (PVA) (Shen et al., 2021) and latex (Samyn et al., 2020). Glassine paper, for example, when coated with PDMS can be used as backings for food wrappers and labels. The manufacturing of glassine paper was first invented by Karlson and patented in 1951 (Karlson, 1951). Most of the lignin in the wood pulp was removed but the hemicellulose content is retained. According to a review by Deshwal et al. (2019), fillers such as titanium dioxide can be incorporated into the pulp to enhance opacity of glassine paper while plasticizers can improve toughness. Subject to the prolonged treatment process during the production of glassine paper will shorten the fibres that help to improve the smoothness of the surface (Trivedi et al., 1979). The application of PDMS gives special characteristics and advantages to glassine paper; however, the major drawback is that they are not suitable to be recycled not only because of the extremely short fibre but also due to the presence of coating. The thermal breakdown of PDMS results in the emission of cyclosiloxane (Zielecka et al., 2020) and the impurities in the form of oligomers can be released into the environment through waste-gases, wastewater and solid waste, eventually entering the food chain and being ingested by both humans and animals (Xiang et al., 2021). Hence, recovery of valuable material from PDMS-coated glassine wastepaper might provide a potential source for the production of microcrystalline cellulose (MCC) in order to utilize the benefits that are offered by this cellulose-rich biomass.

Cellulose has captured the interests of many industries due to its attractive properties attributed to its repetitive chains arrangements and the presence of functional groups in the structure (Riseh et al., 2024). Specifically, MCC is categorized under nanostructured materials with various size, morphology and other characteristics depending on the source of cellulose and extraction conditions (Trache et al., 2020). MCC is a biodegradable material has drawn attention in food industries due to its safe use as a functional food or dietary fiber (Nsor-Atindana et al., 2017) and emulsion stabilizer (Schvartz and Shoseyov, 2022). Due to its poor solubility, MCC is suitable as an excipient (Vora and Shah, 2015), filler or binder in compressible tablets (Agboeze et al., 2022) and internal lubricants (Backere et al., 2022) in pharmaceutical. The three hydroxyl groups per anhydroglucose unit in chains of cellulose makes MCC hydrophilic in nature and strongly interact with water, hence acting as a water reservoir in cement due to its high-water retention capability. The retained water in cement matrix will be released when the free water is diminished during hydration process (Wu et al., 2021) thus improves the mechanical properties of cement (Çavdar et al., 2022). In addition, having abundance of hydroxyl groups on the surface of MCC gives a potential advantage as an adsorbent by interacting effectively with pollutants, allowing them to be removed them from water (Mhike et al., 2023). The production of MCC can be derived from any potential sources with high cellulose content. Lignocellulosic biomass is among the most popular starting materials used in producing the white, odourless and crystalline powder of MCC. Industrial waste such as waste cotton fabrics (Shi et al., 2018), tobacco waste including related tobacco product (W. Salem et al., 2016), rice husk (Nur Hanani et al., 2017) and wastepaper (Uyigue and Okwonna, 2013) have been utilized as a source material for the MCC production.

Recent research has explored innovative methods for extracting cellulose from wastepaper, highlighting its potential as a sustainable resource. One notable study focused on using office wastepaper as a feedstock for cellulose extraction. This process involved an alkali treatment followed by chlorine-free bleaching and acid hydrolysis, resulting in the production of cellulose suitable for creating polyvinyl alcohol (PVA)-starch/cellulose-based biocomposites (Mohammed Irfan et al., 2023). Another research by Lei et al. (2019) focused on extracting cellulose nanocrystals from office wastepaper to reinforce polyurethane, enhancing its thermal and thermo-mechanical properties. A study by Hafid et al. (2023) investigated the extraction of cellulose from gloss art paper (GAP) waste using ultrasonic homogenization. The process improved the particle size, crystallinity and thermal stability of the extracted cellulose, making it suitable for reinforcing starch films in packaging materials. Secondary paper waste has been successfully used to extract cellulose nanocrystals through hydrolysis, resulting in enhanced physical properties, such as increased tear resistance and improved burst indices when added during papermaking processes (Egamberdiev and Norboyev, 2022). Furthermore, Sridhar and collegue (2020), developed a novel method using NaOH/urethane aqueous system to extract microfibrillated cellulose from wastepaper. This method proved effective in removing lead from contaminated water, showcasing the potential of cellulose-based materials in environmental remediation efforts.

Research has also increasingly focused on extracting MCC from wastepaper, with an emphasis on environmentally friendly methods and high-value applications. The common practice in producing MCC from any lignocellulosic materials are delignification, bleaching and hydrolysis. Several methods have been developed for extracting MCC, with acid hydrolysis being the most common due to its ability to yield highly crystalline material. A study investigated the characterization of MCC obtained from paper sludge using different acid concentrations (Zaki et al., 2022). This study found that using a 3.0 M acid concentration achieved the highest crystallinity index, suggesting potential applications in film packaging due to its UV protection properties. However, the extraction of MCC without using traditional acid hydrolysis with sulfuric acid (H_2SO_4) has been explored through various innovative techniques to provide more sustainable and environmentally friendly alternatives to conventional acid hydrolysis, which generate more hazardous waste (Xiu et al., 2019). Hosseinzadeh et al., 2024 developed a novel method for extraction from sugarcane bagasse involves using gaseous hydrochloric acid (HCl) as a milder and greener alternative. R. H. Rana et al. (2022) reported that MCC with desirable tableting properties can be produced without the conventional acid hydrolysis acid by pretreating wastepaper with a chelating agent followed by pulping, bleaching and hydrothermal degradation. The hydrothermal process at high temperature has been previously proven by

Trisant et al. (2020) as an effective method in extracting MCC without the need of acid hydrolysis. The hydroxyl and hypomethyl group in the amorphous is removed at temperature of 120 °C and 140 °C (Zhang et al., 2022). Silvia & Maharani (2023) discovered that enzymatic hydrolysis using cellulase enzyme derived from a microorganism *Trichoderma viride*, effectively to produce MCC from rice straw. Several mechanisms have been described for the cellulose glycosidic bond cleavage such as transglycosylation, ring contcation, glycolysis, ring fragmentation and atom number identification, as highlighted by (Zhu et al., 2017). Furthermore, it was found that prolong alkaline pretreatment may contribute to the dissolution of amorphous cellulose (Bali et al., 2015; Junadi et al., 2019).

The extraction of MCC from PDMS-coated glassine wastepaper has not been addressed or reported by other researcher. This study, therefore, aims to introduce a method for recovering MCC from PDMS-coated glassine wastepaper, focusing on two main objectives: to remove the PDMS coating and to extract MCC. The extracted MCC samples are then characterized qualitatively and quantitatively, with the characterization data compared to that of commercial MCC to evaluate the quality and effectiveness of the extraction process.

2. Experimental section

2.1. Materials

PDMS-coated glassine wastepaper was sourced from a labelling company for use as the raw material in this study. The extraction of MCC was conducted using analytical-grade reagents. Sodium hydroxide (NaOH) with 99% purity was supplied by Merck and sodium hypochlorite (NaOCl), with 10% concentration obtained from QRec. All chemicals were used directly as supplied, without any pretreatment.

2.2. Extraction of microcrystalline cellulose

The PDMS-coated glassine wastepaper was first cut into small pieces and boiled in distilled water for 1 h to remove impurities and soften the paper fibre. After boiling, the paper was blended to form a thick slurry, which was then rinsed multiple times with distilled water. The slurry underwent pre-treatment by boiling with 5% (w/v) NaOH for 3 h and subsequently washed with distilled water until pH 7 was achieved as indicated by the litmus paper. Following the pre-treatment, the neutralized slurry was subjected to treatment with varying concentrations of NaOCl, ranging from 1 v/v% to 2 v/v%, and further increase up to 3 v/v% under vigorous stirring for 2 h. The reaction was quenched by adding distilled water, and the slurry was washed until the solution reached a pH of 7. The resulting sediment was freeze-dried completely before undergoing further characterization. The yield of MCC obtained from the process was calculated using Equation (1):

$$\text{Yield } (\%) = \frac{\text{Weight of dried cellulose}}{\text{Weight of wastepaper}} \text{ x } 100\% \quad \text{Eq. 1}$$

2.3. Physicochemical characterization

The total Si concentrations of the effluent from alkaline treatment at different treatment time were determined by inductively coupled plasma – optical emission spectroscopy (ICP-OES) (model Avio 200; PerkinElmer). The extracted cellulose was identified using Fourier Transform Infrared spectroscopy with attenuated total reflectance technique (ATR-FTIR) (model Frontier; PerkinElmer) in the range of 4000-650 cm^{-1}. The crystallinity was analyzed *via* X-ray diffractometer (XRD) (model Empyrean; PANalytical) in the 2θ angle range of 5° to 50°. Calculation of the crystallinity index (CrI) was determined based on Segal et al. (1959) (Equation (2)).

$$\text{Crystallinity Index, } CrI = \frac{(I_{002}\text{-}I_{AM})}{I_{002}} \; x \; 100\% \quad \text{Eq. 2}$$

Where CrI denotes the degree of crystallinity (%), ($I_{002} - I_{AM}$) is the intensity of the crystalline peak, I_{002} represents total intensity of 002 lattice diffraction while I_{AM} is the diffraction intensity for the amorphous part. The crystallite sizes of extracted MCC of different bleach concentration were estimated using Scherrer equation (Equation (3)):

$$\text{Scherrer equation, } D = \frac{K\lambda}{\beta \cos\theta} \quad \text{Eq. 3}$$

where $K = 0.94$, λ is the x-ray wavelength of 1.5406 Å, β corresponds to the full width at half maximum (FWHM) measures in radian located at any peak position (2θ) in the spectrum. The thermal stability of the extracted cellulose was studied using thermal gravimetric analysis (TGA) (model DTA-TG DTG-60H; Shimadzu) with temperature ranging from 30 °C to 800 °C at 10 °C/min of heating rate under nitrogen atmosphere with flow rate of 200 ml/min. The physical properties of MCC were studied by observing the morphology and particle dimension of the samples using Scanning Electron Microscope (SEM) (model JSM-IT200LV; Jeol Ltd.) where the samples were sputter coated with platinum to avoid charging. To further investigate the particle size, a selected MCC sample was subjected to particle size distribution analysis using Shimadzu SALD-2300 particle size analyser, applying a refractive index of 1.55 as per method by Gaudreault et al. (2005). The result was then compared with those of commercial MCC. The images and dimensions of selected MCC sample and commercial MCC were also obtained using high resolution transmission electron microscopy (HR-TEM) with Hitachi HT7700 at an accelerating voltage of 120 kV.

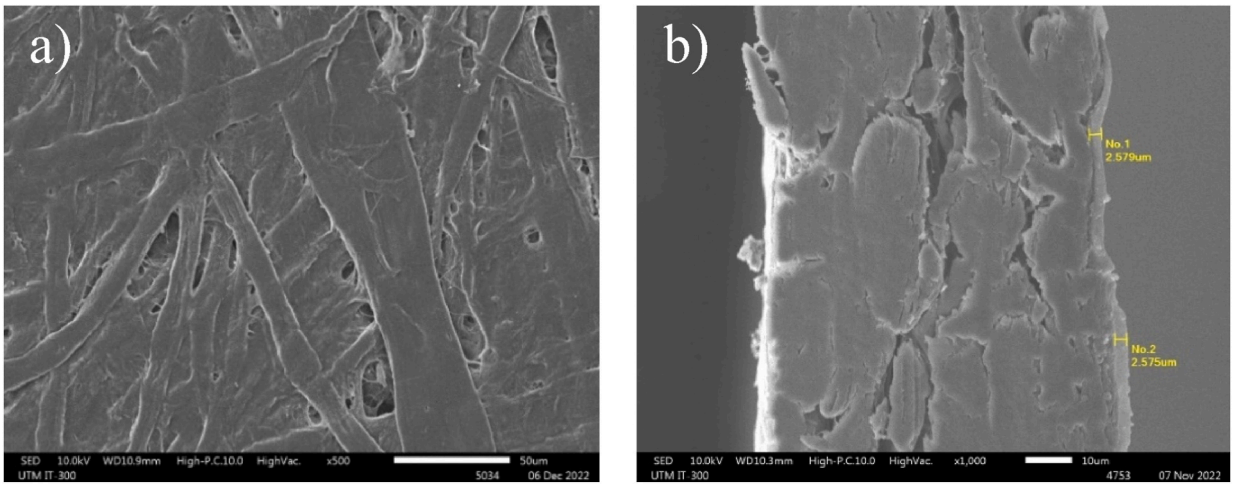

Fig. 1. SEM micrographs of: a) paper-side of PDMS-coated wastepaper; and b) cross section image of coated wastepaper with approximate thickness of 2.575–2.579 μm.

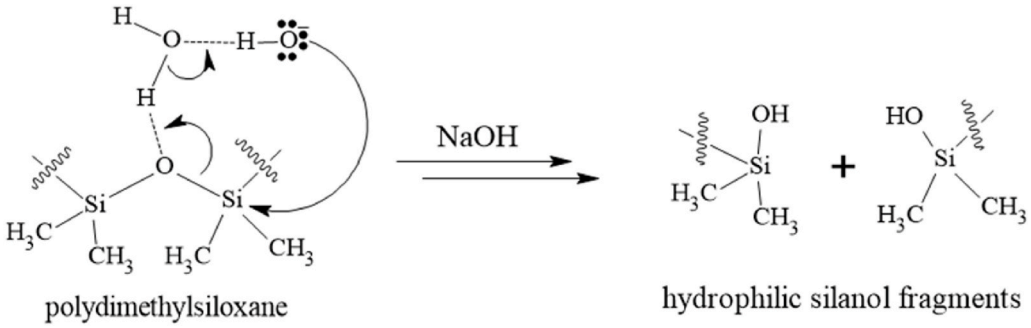

Fig. 2. Possible reaction mechanism of PDMS degradation by NaOH adapted from Kaden et al. (2017).

3. Results and discussion

3.1. Morphology of PDMS-coated glassine wastepaper

The morphology and the coating layer of PDMS on wastepaper were examined using SEM as depicted in Fig. 1. The micrograph reveals a densely packed structure of paper fibers with various sizes and orientations, indicative of the low porosity characteristic of the paper sample employed for MCC extraction (Vicente et al., 2017). The presence of a high concentration of small-sized fibers, ranging from 3 to 10 μm in width, effectively fills the gaps between the larger fibers (>30 μm). No aggregation observed on the surface or in between the paper fibers, suggesting the absence of filler on the PDMS-coated glassine wastepaper. According to Han et al. (2020), fillers such as calcium carbonate can be distinctly identified by their aggregation around paper fibers. The application of PDMS coating layer serves to enhance the hydrophobicity of the paper. Line scan results indicate the presence of a thin coating layer, with a thickness ranging from 2.575 to 2.579 μm, observable in the paper's cross-sectional image. Söz (2022), expanding on the research by Krumpfer and McCarthy (2011), described a potential interaction mechanism between paper and PDMS. The mechanism suggests that Si–*O*–C bonds are formed when the siloxane units of PDMS interact with the hydroxyl groups on paper surface, facilitated by adequate heat treatment.

3.2. Alkaline treatment

The PDMS-coated wastepaper was subjected to 5% NaOH solution for 3 h. The effect of this alkaline treatment on the paper coating and morphology were assessed.

3.2.1. Effect of alkaline treatment on paper coating

Alkaline treatment is a crucial process in the extraction of cellulose and the removal of PDMS from various raw materials. This method involves the use of an alkaline solution, NaOH, to break down and dissolve non-cellulosic components such as lignin,

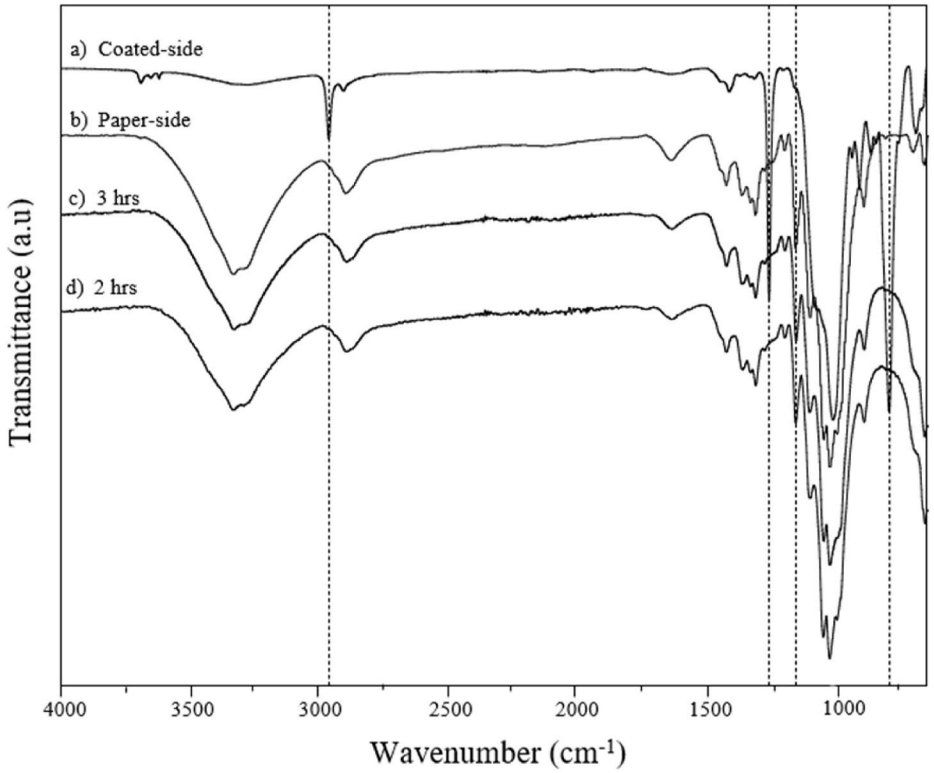

Fig. 3. FTIR spectra of paper pulp after 2 h and 3 h of alkaline treatment with 5% NaOH.

hemicellulose and other impurities (Lei et al., 2019). In the context of PDMS-coated materials, alkaline treatment is particularly effective in hydrolysing and removing the PDMS layer (Örn, 2019). The high pH environment disrupts the siloxane bonds in PDMS, facilitating its removal and leaving behind purified cellulose fibers. This dual functionality of alkaline treatment not only purifies the cellulose but also ensures the effective removal of synthetic coatings like PDMS, making the cellulose suitable for various industrial applications.

Under alkaline conditions, PDMS is hydrolysed into hydrophilic compounds such as siloxanols. According to Kaden et al. (2017), both acidic or alkaline pH levels promote chemical degradation of PDMS. Fig. 2 shows the possible reaction mechanism of PDMS degradation by NaOH. The reaction of PDMS with NaOH involves the nucleophilic hydroxide ion, OH^-, attacking the silicon atoms, Si, in the siloxane bonds, leading to the formation of a pentavalent silicon intermediate. The intermediate undergoes a transition state stabilized by hydrogen bonding, leading to the cleavage of the Si–O bonds in the polymer chain. As a result, the siloxane bonds break down, producing smaller molecules with silanol groups (Si–OH), effectively degrading the PDMS into more hydrophilic silanol-containing fragments. The extent of PDMS removal during alkaline treatment is influenced by the reaction time whereby longer reaction time allow for more thorough etching or removal of the polymer (Örn, 2019).

Fig. 3 shows the FTIR spectra of paper pulp subjected to a 5% NaOH of alkaline treatment, comparing the effects on both the coated-side and paper-side at different treatment time of 2 h and 3 h. The variations in peak intensity and shifts reveal changes in the cellulosic and hemicellulosic components of PDMS-coated glassine wastepaper pulp. A broad peak around 3300-3400 cm^{-1} and 2900 cm^{-1} were observed in all samples except for coated side of the PDMS-coated glassine wastepaper, associated with O–H and C–H stretching vibrations which typically found in lignocellulosic materials. However, the absorption peak of lignin was not detected in both paper-side and coated-side of PDMS-coated glassine wastepaper. The absence of the characteristic lignin peak at 1530 cm^{-1} assigned to C═C aromatic ring vibration (Kostryukov et al., 2023) confirms that the lignin in PDMS-coated glassine wastepaper is very minimal. Upon alkaline treatment with NaOH regardless of duration, a reduction in peak intensity was noted at 1157 cm^{-1} and 897 cm^{-1}, particularly more pronounced in the paper-side of the PDMS-coated glassine wastepaper. These two peaks represent C–*O*–C vibrations of arabinosyl units in hemicellulose (Haryanti et al., 2022) and β-glycosidic linkages between the xylose units in hemicellulose (Flórez-Pardo et al., 2019), respectively. The decrease in these peak intensity for alkaline treated PDMS-coated wastepaper pulp suggests the intermolecular degradation in the hemicellulose structure. These changes are the crucial factor that supports the removal of hemicellulose after the alkali treatment.

Furthermore, FTIR spectra of alkaline-treated PDMS-coated wastepaper pulp for 2 h and 3 h of reaction time showed the absence of three (3) distinct peaks located at 795 cm^{-1}, 1256 cm^{-1} 2960 cm^{-1}. These peaks correspond to the asymmetric CH_3 stretching in Si–CH_3, deformation of CH_3 in Si–CH_3 and Si–C stretching in Si–CH_3, respectively. Preliminary analysis using FTIR confirmed that the three (3) significant sharp peaks are characteristics of PDMS. Another notable peak for PDMS, corresponding to Si–*O*–Si stretching,

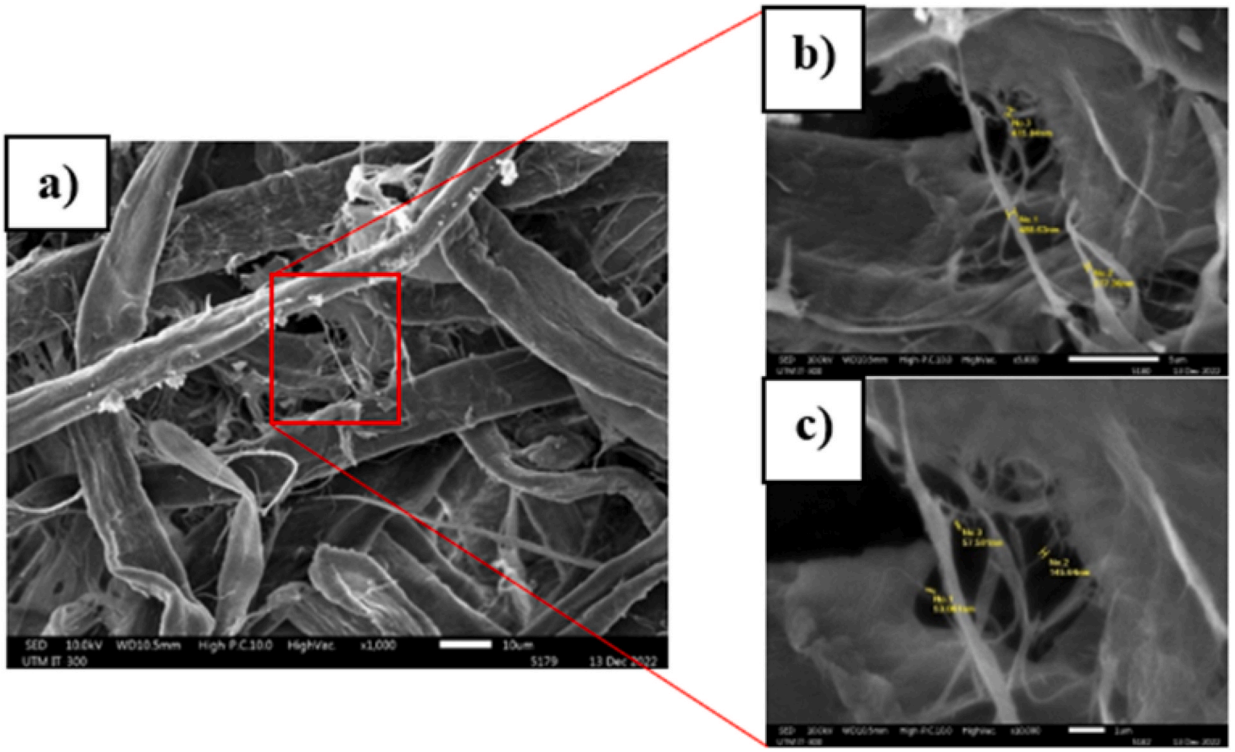

Fig. 4. SEM micrographs of the (a) alkaline-treated paper fiber, (b) and (c) zoom-in of the area marked in (a).

appears at 1012-1076 cm^{-1} as identified by Johnson *et al.* (2013). The findings indicate that the chemical degradation of PDMS is effectively achieved under alkaline conditions, with the complete removal of characteristic PDMS peaks in the FTIR spectra after sufficient reaction time. This confirms the efficiency of the alkaline treatment in breaking down PDMS and converting it into hydrophilic compounds, thereby enabling its removal from the treated materials.

In addition, the efficiency of PDMS removal by NaOH at different reaction time was quantified using ICP-OES where the average silicon (Si) concentration for each reaction time was measured. The findings demonstrated that extending the reaction time to 3 h led to a higher Si concentration (57.53 mgL^{-1}) in the treatment effluent compared to 33.21 mgL^{-1} observed after 2 h reaction time. While extended alkaline treatment is expected to remove a greater amount of Si, it can also potentially damage the cellulose structure (Sriprom et al., 2022). Furthermore, as the reaction time increases, the paper slurry becomes thicker due to vaporization of liquid, thereby limiting the stirring motion. Hence, an optimal reaction time of 3 h is recommended for alkaline treatment. Additionally, during the bleaching step, a residual Si concentration of 1.52 mgL^{-1} was released into the aqueous phase as a result of PDMS degradation, indicating that Si removal also occurred during the bleaching process.

3.2.2. *Effect of alkaline treatment on the morphology of paper fiber*

Fig. 4 presents the SEM micrograph of the paper fiber after 3 h of alkaline treatment with NaOH. The alkaline treatment has effectively disrupted the compact fiber bundles, breaking them down into individual cellulose microfibrils with diameters ranging from 100 to 500 nm. Alkaline treatment significantly increases the surface area of lignocellulosic biomass through several mechanism. Primarily, NaOH disrupts the hemicellulose and lignin matrix, that contribute to the recalcitrance of lignocellulose. This process breaks down the complex polymer into simpler molecules such as monosaccharides and oligosaccharides. The removal of these components not only increases the porosity but also inflates the cellulose structure, making it more accessible for further chemical reaction (Junior et al., 2013).

NaOH plays a significant role in the dissolution and structural modification of hemicellulose. Hemicellulose, characterized by its amorphous and highly branched structure, is particularly vulnerable to alkali attacks (Barman et al., 2020). When NaOH is introduced in the solution, it interacts with the cellulose and hemicellulose components of the pulp, facilitating the separation and dissolution processes. NaOH can break the inter and intramolecular hydrogen bonds within the cellulose and hemicellulose structures, thereby enhancing their solubility (Qin et al., 2021; Rodrigues et al., 2023). Moreover, the alkaline treatment by NaOH causes the breakdown of the intermolecular ester bonds between lignin and hemicellulose as well as between lignin and cellulose, leading to their removal and thus exposing the cellulose fibers (Abolore et al., 2024; Yang et al., 2021). A high concentration of NaOH causes disruption in the crystalline regions of cellulose, leading to an increase in its solubility results in the treatment solution. This increased solubility results in the cellulose dissolving more readily, which ultimately decreases the yield of the cellulose fiber (Sayakulu and Soloi, 2022).

This defibrillation and disruption of the hydrogen bonding network are achieved through alkaline treatment, commonly known as

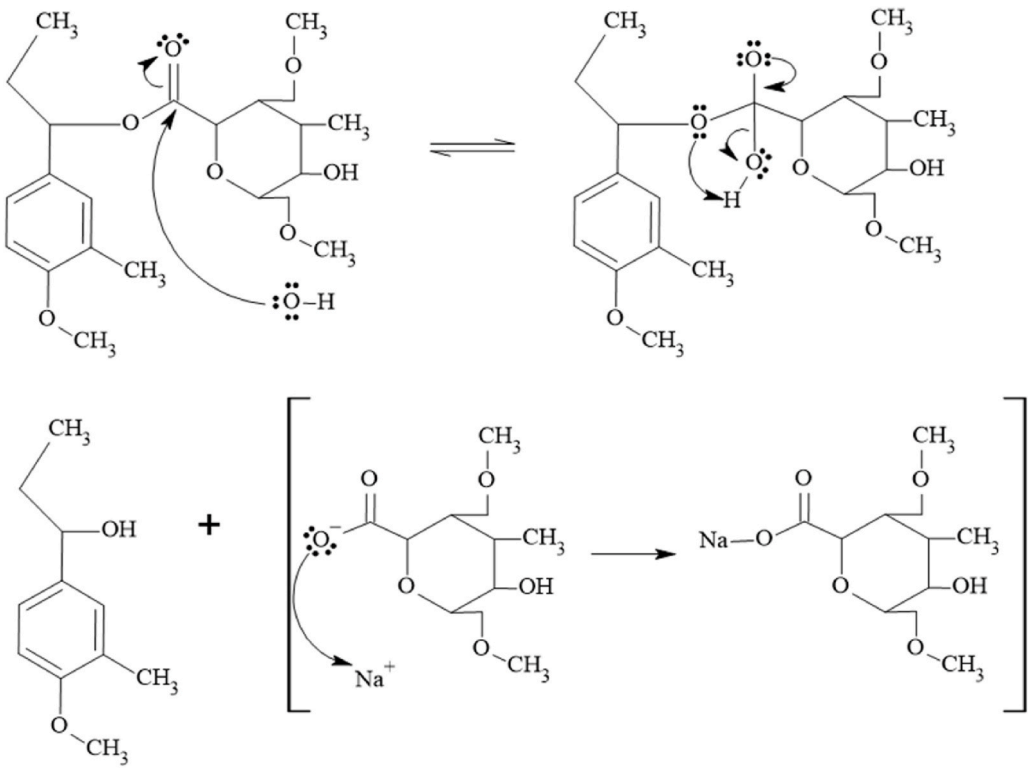

Fig. 5. Reaction mechanism of hydrolysis by NaOH of ester bond in lignocellulose. The lignocellulose structure was adapted from Barman et al. (2020).

mercerization (Verma and Goh, 2021). Additionally, NaOH modifies the chemical structure of the fibers by converting hydroxyl, –OH groups to sodium alkoxide, -ONa$^+$ groups (Akram Khan et al., 2011). The reaction mechanism of alkaline treatment by NaOH, as illustrated in Fig. 5, involves a series of chemical interactions initiated by the OH$^-$. The OH$^-$ ion specifically targets and attacks the carbon atom present in the ester bond. These ester bonds are integral connections that can occur in various configurations: between lignin and carbohydrate molecules, linking two lignin components together, or joining two carbohydrate components (Modenbach and Nokes, 2014). The rapid reaction involving the resulting alkoxide acting as a base to deprotonate the carboxylic acid, leading to the irreversible hydrolysis of the ester bond, significantly weaken the structural integrity of lignocellulose. Alkoxide is essential in the degradation of hemicellulose in NaOH by aiding the breakdown of hemicellulose into smaller molecular components. Additionally, sodium carboxylate formed during the degradation of hemicellulose is water-soluble, facilitating its dissolution in aqueous NaOH solutions (Budtova and Navard, 2016).

3.3. *Bleaching treatment*

The next step in the extraction of MCC involves a bleaching process using NaOCl resulting in a white, powdery MCC. All MCC samples are denoted as MCC1.0%, MCC1.2%, MCC1.4%, MCC1.6%, MCC1.8%, MCC2.0%, MCC2.5% and MCC3.0% according to NaOCl concentration used. Bleaching treatment using NaOCl plays an important role in the extraction of MCC by effectively removing any residual hemicellulose and lignin from cellulose fibers. The concentration of NaOCl significantly impacts the extraction of MCC by influencing the removal impurities, the integrity of cellulose fibers and the overall yield. The optimal NaOCl concentration can vary depending on the source material, as different materials contain varying levels of hemicellulose and lignin, affecting their response to bleaching. For instance, a 5% NaOCl concentration is used for rice husk (Ahmad et al., 2016), 4% for Lembang Plant (Sayakulu and Soloi, 2022) and 3.5% for tapioca solid waste (Ansharullah et al., 2020). Higher concentrations of NaOCl are more effective at removing impurities, leading to a purer MCC product. However, these higher concentrations can also cause greater degradation of the cellulose fibers, reducing both the quality and yield of MCC. Specifically, as the concentration of NaOCl increases, the yield of MCC tends to decrease because of the more aggressive bleaching process breaks down the cellulose chains. Finding the optimal concentration is crucial; it must be high enough to remove impurities but low enough to preserve the cellulose fibers' integrity and maximize yield. Therefore, controlling the NaOCl concentration carefully is essential to balance impurity removal with cellulose fiber preservation, optimizing both yield and quality of MCC.

In this study, the wastepaper used in this study contains 22.64% hemicellulose and only 3.02% lignin. Due to the low lignin content in the wastepaper, less protection is needed against cellulose degradation. While lignin provides rigidity and structural support to plant

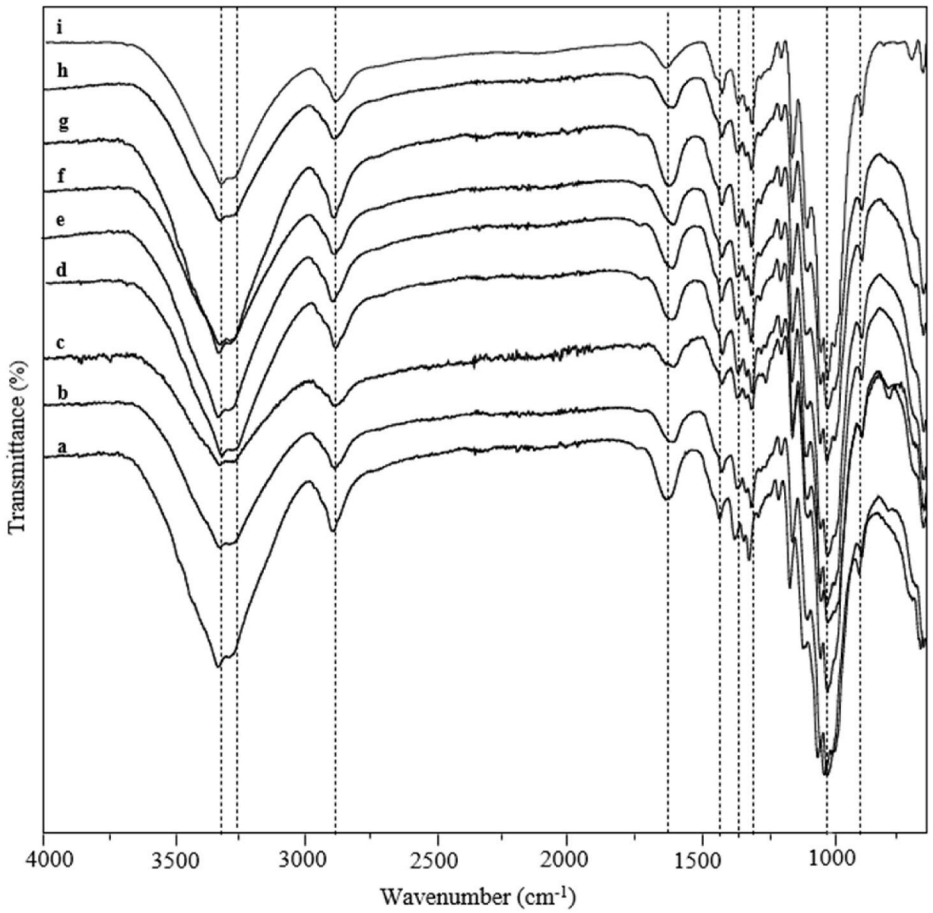

Fig. 6. FTIR spectra of MCCs extracted from PDMS-coated wastepaper under different NaOCl concentration: a) 1.0%, b) 1.2%, c) 1.4%, d) 1.6%, e) 1.8%, f) 2.0%, g) 2.5%, h) 3.0% and i) commercial MCC.

cell walls, it also protects cellulose fibers from degradation, hence act as a shield, preventing acute degradation of the fibers during bleaching (Gierer, 1982). This allows for the use of lower concentrations of NaOCl as the bleaching agent, under controlled conditions and the findings of this study validate this approach. As the concentration of NaOCl increases, the yield of MCC decreases. Starting at 1.0% NaOCl, the yield is 58.4% but it gradually declines as the concentration increases to 3.0%, reaching its lowest at 42.7%. This trend indicates that higher NaOCl concentrations result in lower MCC yields. The data suggests that the reduction in yield at higher concentration of NaOCl could be due to over-oxidation or degradation of the cellulose. Delignification through alkaline and bleaching treatments is a critical process in the modification of lignocellulosic materials, often leading to significant weight loss. The weight reduction is primarily due to the dissolution of hemicellulose and lignin, along with the degradation of the PDMS coating. The breakdown of these two key lignocellulosic components from the starting materials results in a notable decrease in yield and contributes to the loss of pulp strength (Esteves et al., 2022).

As the bleaching condition is getting more severe by using higher NaOCl concentration, higher temperature and a longer bleaching time, the extracted cellulose will be affected due to the kinetic effects and collision theory (Peleg, 2023). NaOCl concentration and temperature exhibited significant impact on the quality of cellulose whereby excessive bleaching conditions caused severe oxidation of celluloses and significantly reduced their dimension. Therefore, the reaction condition needs to be controlled to keep the degradation of cellulose at a minimum. Degradation of cellulose might occur when the glycosidic bond in cellulose is ruptured (Aridi et al., 2021) and oxidized by NaOCl thus lowering the molecular weight of the cellulose and increase solubility (Aurelia et al., 2019; Garrido et al., 2014). However, dissolution of cellulose will not occur if the treatment temperature used is lower than its degradation temperature due to the strong intra and intermolecular hydrogen bonding within the cellulose structure (Sayakulu and Soloi, 2022). Another external factor affecting the percentage yield is the loss through washing during the neutralization stage.

3.3.1. Dissolution of NaOCl in water

When NaOCl is introduced into water, it undergoes several series of reactions. As shown in Equation (4), NaOCl reacts with water to form sodium ions, Na^+ and hypochlorous acid, HOCl. The dissociation of NaOCl creates a dynamic equilibrium of NaOH and hypochlorous acid (HOCl). In aqueous system, HOCl dissociates into hydrogen ion, H^+ and hypochlorite ion, OCl^-, where chlorate ion,

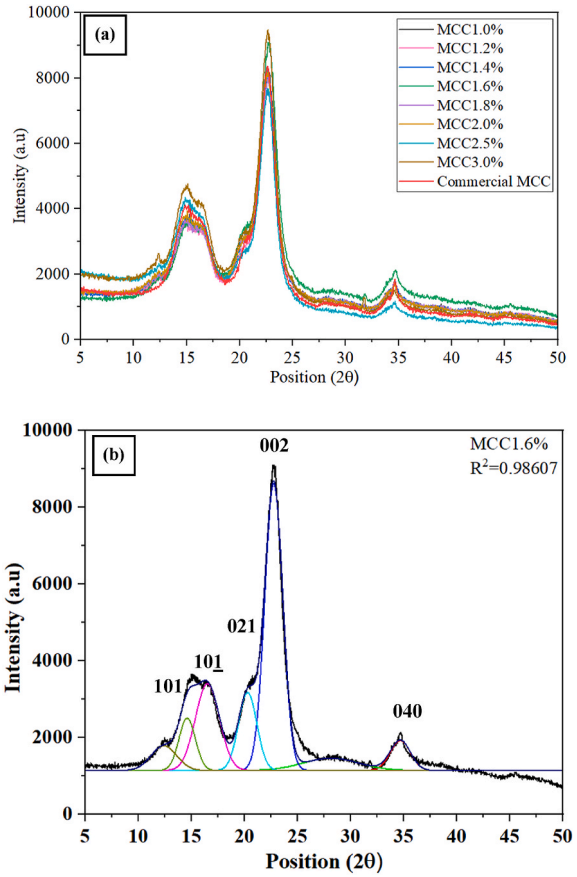

Fig. 7. XRD diffractograms of (a) extracted samples and commercial MCC; and (b) peak deconvolution for MCC1.6%.

ClO_3^- is produced resulting from the reaction of OCl^- in a fast rate. As highlighted by Gordon et al. (1997), NaOCl is a strong oxidizing agent due to the rapid formation of chlorate ion (ClO_3^-) with high oxidation number in aqueous.

$$\begin{aligned} &NaOCl + H_2O \rightarrow HOCl + Na^+(OH^-) \\ &HOCl \rightarrow H^+ + OCl^- \\ &OCl^- + OCl^- \rightarrow ClO_{2^-} + Cl^- \left(\begin{matrix}\text{Slower}\\ \text{step}\end{matrix}\right) \\ &OCl^- + ClO_{2^-} \rightarrow ClO_{3^-} + Cl^- \left(\begin{matrix}\text{Faster}\\ \text{step}\end{matrix}\right) \end{aligned} \quad (4)$$

The oxidation number of chloride in ClO_3^- in the faster step is +5, requiring more electrons for stabilization. This suggests that ClO_3^- initially attack the remaining lignin and hemicelluloses prior to cellulose especially in the amorphous regions which are easier to break down and hydrolyze chemically than the crystalline regions (Isroi and Cifriadi, 2018). Referring to proposed reaction mechanism of lignin oxidized by NaOCl, as described by R. Wang et al. (2019), HOCl formed in aqueous solution act as an electrophile that target the ortho positions of –OR group of lignin to eliminate H^+ ions. As the oxidation process continues, benzenediol will be oxidized to break the ring structure and finally converted into carboxyl and CO_2. According to Estrela et al. (2002), HOCl and OCl^{-1} can lead to hydrolysis and increase in temperature of NaOCl solution can enhance its ability to dissolve organic matter (Stojicic et al., 2010). Additionally, Sang et al. (2017) highlighted that the amorphous region of cellulose can be accessed and readily degraded by NaOCl to produce dissolved fragments of cellulose. From the FTIR analysis as shown in Fig. 3, the intensity of the lignin peak at 1530 cm^{-1} is very weak. With the advantage of NaOCl as described by Sang et al. (2017) and the low content of lignin in PDMS-coated glassine wastepaper, this will create a favourable condition for NaOCl to degrade the amorphous region in cellulose.

3.4. Characterization of extracted MCC

3.4.1. Functional group analysis using ATR-FTIR

The common cellulose FTIR spectra are characterized by four important regions: (1) OH stretching region (3700-3000 cm^{-1}), (2) CH stretching region (3000-2700 cm^{-1}), (3) OH bending region (1800-1300 cm^{-1}) and (4) fingerprint region with multiple C–O

Table 1
FTIR and XRD data for extracted and commercial MCC.

Sample	FTIR		XRD	
	LOI	TCI	Crystallinity Index (%)	Average Crystallite Size (nm)
MCC1.0%	0.62	1.08	77.86	3.39
MCC1.2%	0.57	1.24	78.85	3.38
MCC1.4%	0.55	1.05	77.66	3.36
MCC1.6%	0.52	1.26	78.90	3.33
MCC1.8%	0.49	1.17	77.72	3.42
MCC2.0%	0.42	1.22	77.92	3.32
MCC2.5%	0.33	1.19	76.99	3.37
MCC3.0%	0.39	1.14	76.53	3.35
Commercial MCC	1.02	1.01	79.24	3.78

vibrations (1250-850 cm^{-1}) as shown in Fig. 6. A broad OH stretching band ranging from 3644 to 3000 cm^{-1} is observed across all samples, comparable with a prominent peak at 3332 cm^{-1} and a weak shoulder at 3274 cm^{-1} in commercial MCC, labelled as commercial MCC. This band is attributed to the intermolecular and intramolecular O–H stretching vibrations, which are essential for understanding the hydrogen bonding network in cellulose. The broad nature of this band indicates extensive hydrogen bonding as noted by Li et al. (2023). The CH asymmetric band is observed around 2900 cm^{-1} corresponding to the C–H stretching vibrations within the cellulose molecule. These vibrations are important for understanding the cellulose backbone's structural integrity and composition. A band observed at 1622 cm^{-1} is attributed to the bending vibrations of water molecules. The position of this band can shift to a lower wavenumber, reflecting stronger interactions between water molecules and the hydrogen bonding network in cellulose. Such shifts indicate changes in the hydration state and the strength of hydrogen bonds within the cellulose matrix (Hong et al., 2021; Seki et al., 2020). Another band related to CH vibration, the CH asymmetric deformation at 1366 cm^{-1} represents the C–H bending vibrations. The fingerprint region at 1250-850 cm^{-1} is known for its complex patterns unique to cellulose. This region contains multiple bands related to C–O stretching and C–H bending vibrations, which are important for identifying the unique structural features of cellulose. At wavenumber of 897–900 cm^{-1}, the band is assigned to CH deformation of β-glycosidic linkages and the amorphous structure of cellulose. The reduction in the intensity of the peak at 897 cm^{-1} could be indicative of an increase in the crystallinity of the obtained MCC samples, as highlighted by K. S. Salem et al. (2023) and Wahlström et al. (2020).

The intensity of the band at 1366 cm^{-1} and 2900 cm^{-1} are essential for calculating the Total Crystalline Index (TCI). The TCI is derived from the absorbance ratio of the CH bending vibrations band at 1366 cm^{-1} to CH stretching band at 2900 cm^{-1}. This ratio indicates the degree of crystallinity regions, correlating with a more ordered and stable cellulose structure. A higher TCI value indicates a higher degree of crystallinity, reflecting a more ordered cellulose structure. Another indicative band of the crystalline structure within cellulose is at 1425-1430 cm^{-1}. The intensity of this band reflects the amount of crystalline cellulose present, with higher intensities signifying a more ordered crystalline structure. The absorbance of the band at 897-900 cm^{-1} is taken for determining the Lateral Order Index (LOI). The LOI value is derived from the absorbance ratio of the bands at 1425-1430 cm^{-1} and 897-900 cm^{-1}. It explains the overall degree of order in cellulose, with higher LOI values indicating a more organized arrangement of cellulose chains (Cichosz and Masek, 2020).

3.4.2. Crystallinity studies of MCC

Fig. 7(a) displays the XRD patterns of all extracted and commercial MCC samples. The figure clearly shows that MCC extracted at various NaOCl concentrations are crystalline, matching the crystallinity of commercial MCC. The diffraction pattern of MCC is characterized by a major peak approximately 22.7° (002) and a shoulder peak at 20° (021), which indicates the polymorph of cellulose I crystalline structure. In Fig. 7(b), the peak deconvolution of MCC1.6% diffraction spectrum shows distinct diffraction peaks corresponding to the cellulose I polymorph. The major peaks at approximately 2θ of 16° (101), 20° (021), 22.7° (002) and 34.5° (040) confirm the presence of crystalline cellulose. So-yoon Park et al. (2024) reported the same findings for MCC extracted from pistachio shells with 2θ around 14.9–16.2°, 22.1–22.3° and 34.5°. As highlighted by Wei & Li (2016), the CrI, reflects the proportion of ordered regions within the cellulose structure while *d*-spacing represents the distance between parallel atomic planes in a crystal, commonly referred to the interplanar distance and can be calculated according to Bragg's law as shown in Equation (5):

$$d = \frac{n\lambda}{2 \sin \theta} \quad \text{Equation 5}$$

where λ refers the X-ray wavelength (1.542 Å) and θ denotes the Bragg angle associated with the (002) plane.

MCC treated with 1.6% NaOCl concentration shows the highest CrI. This suggest that at this concentration the amorphous components were effectively removed while simultaneously preserving the crystalline regions. In terms of *d*-spacing, represented by d_{002}, the data reveals a distinct trend that differs from that of the CrI. The d_{002} parameter reaches its lowest value of 3.91 Å, at NaOCl concentration (1.6%) compared to 3.93 Å for commercial MCC, indicating a densification of the crystalline structure (Howell et al., 2011; Ren et al., 2022). The intermolecular forces between cellulose chains are stronger with decreasing interplanar distance, allowing the cellulose chains to pack more tightly which enhances the overall structural order of the cellulose matrix (Cui et al., 2014). However, as the concentration of NaOCl increases beyond 1.6%, the *d*-spacing begins to increase, indicating the loosening of the

crystalline layers (Arnata et al., 2019; Chen et al., 2016). The higher value of d-spacing shows cellulose structure become less compact due to the swelling of the cellulose resulting from the oxidative effect of NaOCl (T. Wang and Zhao, 2021).

In this study, PDMS-coated glassine paper originally has a crystallinity index of 82.42%. However, when subjected to alkaline and bleach treatment, a noticeable decrease in crystallinity is observed. The observation was also noted by Das et al. (2010) who found that the high crystallinity of filter paper was reduced when exposed to chemical treatment. Table 1 provides a detailed overview of the crystallinity and crystallite size of extracted MCC samples compared to commercial MCC. The crystallinity data derived from FTIR, includes the LOI and TCI, while the crystallinity index is obtained from XRD analysis. These parameters provide insight into the structural order and crystalline content of the cellulose. Furthermore, the table presents the average crystallite size determined by XRD analysis, which indicates the dimensions of the crystalline regions within the MCC samples. The crystallinity index for MCC1.0% is 77.85% and increases slightly to 78.85% for MCC1.2% indicating an initial improvement in crystallinity. However, the crystallinity index values for MCC1.4% to MCC2.0% shows slight fluctuations between 77.66% and 78.90% but remain relatively close to each other. These small variations suggest that within this concentration range, the crystallinity is affected in a controlled manner, with minor differences possibly arising from subtle inconsistencies in the treatment process. A more significant reduction in crystallinity is observed as the NaOCl concentration increases further where the crystallinity index for MCC2.5% and MCC3.0% drops to 76.99% and 76.53%, respectively. The decreasing trend indicates that higher NaOCl concentrations start to adversely affect the crystalline regions and confirms the significant disruption of the crystalline structure at excessive NaOCl levels. When comparing these results with the commercial MCC which has a crystallinity index of 79.24%, it is apparent that the optimally bleached MCC at 1.6% NaOCl concentration displays a marginally lower yet comparable degree of crystallinity. However, as the concentration increases, the difference becomes more significant, with MCC3.0% exhibiting a much lower crystallinity index than the commercial MCC. This highlights that while controlled bleaching can enhance crystallinity to a certain extent, excessive bleaching adversely affects the crystalline structure, leading to a reduction in the overall crystallinity of the material. The crystallinity index from XRD is used to further confirm the crystallinity data obtained through LOI and TCI calculations based on FTIR absorbance values.

The LOI and TCI values collectively reflect the structural and crystalline characteristics of MCC (Poletto et al., 2014; Polettoa et al., 2012). Both values are useful metrics for characterizing the crystallinity properties of MCC using FTIR. The data indicates noticeable variations in the LOI and TCI indices of MCC extracted at different NaOCl concentrations, reflecting significant differences in the structural organization and crystallinity of the MCC. The MCC samples extracted at varying NaOCl concentrations show lower LOI values, ranging from 0.33 to 0.62, and varying TCI values between 1.05 and 1.26. This reflects that extracted MCC has a less ordered structure, consisting of both crystalline and amorphous regions. The combination of high LOI and low TCI in MCC samples suggests that, although the MCC arrangement are well-ordered laterally, the overall structure still contains a significant amount of amorphous regions (Poyraz et al., 2018). The MCC extracted with lowest NaOCl concentration displays the highest LOI of 0.62 among all extracted MCC, accompanied by a low TCI of 1.08, indicating the MCC1.0% has a well-ordered lateral arrangement of cellulose chains but also contains a significant amount of amorphous regions. As the concentration of NaOCl increase up to 3.0%, the LOI decreases, suggesting that the higher NaOCl concentration in the extraction process leads to excessive degradation or disruption of cellulose (Isroi et al., 2017). This elevated concentration likely causes a more severe breakdown of both crystalline and amorphous regions, resulting to a MCC with lower structural order and reduced crystallinity. However, the determination of crystallinity should not be exclusively based on FTIR spectroscopy as this technique provides relative values that reflect contributions from both crystalline and amorphous regions and essentially to corroborate with additional analytical methods such as XRD (Park et al., 2010).

The comparison between extracted MCC and commercial MCC reveals several key differences in terms of crystallinity and structural organization, as revealed by FTIR and XRD analyses. Commercial MCC exhibits a notably higher LOI of 1.02 and TCI of 1.01, which collectively indicate a highly ordered and crystalline structure. This superior crystallinity is further supported by XRD data, where commercial MCC shows the highest crystallinity index of 79.24%. Among the extracted samples, MCC 1.6% stands out with a TCI of 1.26 and a crystallinity index of 78.90%, which are the closest to those of commercial MCC. These values have shown a consistent correlation with the crystallinity index derived from XRD data calculations as demonstrated in the research by Sangian et al. (2018). This indicates that a NaOCl concentration of 1.6% is optimal for preserving the crystalline structure during extraction, resulting in a product with properties that approach those of commercial MCC. When comparing MCC1.6% with commercial MCC, both of which have a comparable XRD crystallinity index, several differences become apparent. MCC1.6% shows a higher TCI of 1.26 whereas commercial MCC has a TCI of 1.01, indicating that MCC1.6% has greater overall crystallinity according to FTIR measurements. On the other hand, commercial MCC has a significantly higher LOI of 1.02 compared to 0.52 for MCC1.6%, indicating better lateral crystalline alignment in commercial MCC. The conclusion that can be drawn from the comparison between MCC1.6% and commercial MCC is that each material exhibits unique strengths in terms of crystallinity characteristics. These differences suggest distinct applications for each material. MCC1.6% with its higher TCI, may be more suitable for applications requiring high stability and uniformity (Zhao et al., 2022). On the contrary, commercial MCC with its superior lateral crystalline alignment and high crystallinity index, might be better suited for applications where enhanced mechanical properties and better structural integrity are crucial (Janmohammadi et al., 2023; Poyraz et al., 2018). The inclusion of highly crystalline cellulose will increase the strength of a biocomposite material (Ahvenainen et al., 2016; Ni'mah et al., 2017).

The crystallite size of MCC significantly influences its physical and chemical properties, making it another important parameter for optimizing MCC for various applications. The extracted MCC samples exhibit average crystallite sizes between 3.32 nm and 3.42 nm, vary slightly among the different concentrations. However, commercial MCC has an average crystallite size of 3.78 nm, which is larger compared to the extracted samples. Smaller crystallite sizes generally result in higher mechanical strength due to the increased density of grain boundaries, which impede dislocation motion, making the material more rigid and resistant to deformation (Stricker and Weygand, 2024). Additionally, MCC with smaller crystallites tend to have higher thermal stability, as increased surface area enhances

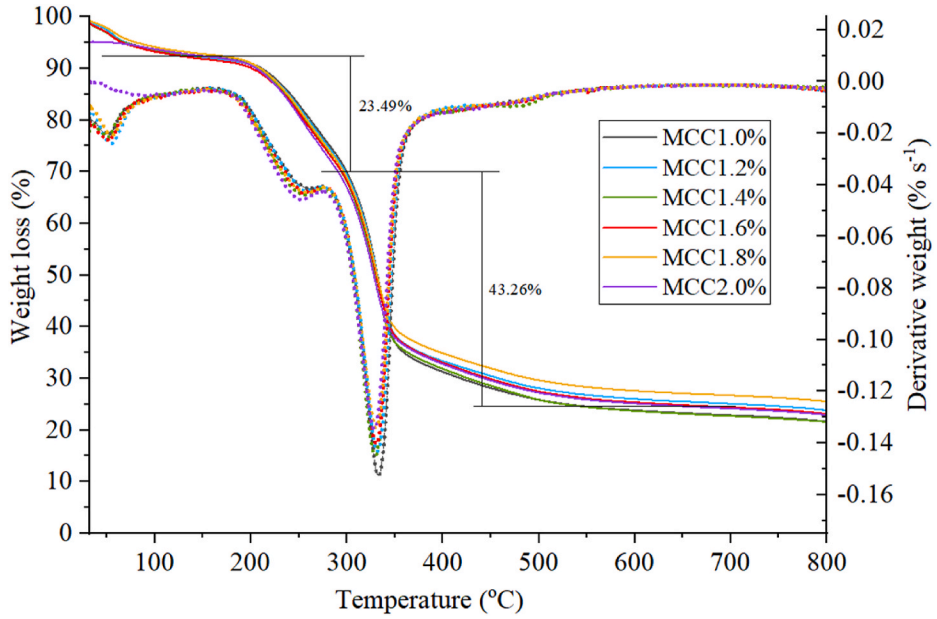

Fig. 8. TGA/DTG curves (shown in solid and dotted lines, respectively) of extracted MCC with NaOCl concentration range of 1.0%–2.0%.

the interaction between cellulose chains, making the material more resistant to thermal degradation (Zhou et al., 2018). Chemically, smaller crystallites exhibit higher reactivity due to a higher surface area-to-volume ratio, which is beneficial in applications requiring efficient chemical modification (Cerro et al., 2020). In pharmaceutical applications, smaller crystallite sizes enhance solubility and dissolution rates, improving the bioavailability of active drugs (Huang et al., 2023). The significant variability of crystallite size of MCC are due to several factors including the inherent properties of cellulose source, the methods employed during extraction and various post-processing conditions. These variations with crystallite sizes can be ranging from as low as 2.40 nm for Lembang (*Typha angustifolia* L.*)* (Adawiyah et al., 2022) to as high as 9.41 nm for oil palm frond (Syamani et al., 2015).

Previous studies have highlighted significant variations in the concentrations of NaOCl, with differences in the resulting crystallinity observed across various sources. Generally, higher concentrations of NaOCl do not necessarily lead to higher crystallinity. For instance, tapioca solid waste treated with 3.5% NaOCl shows the highest crystallinity of 94.16% (Ansharullah et al., 2020), whereas rice husk with a higher concentration of 5% NaOCl exhibits a much lower crystallinity of 63.90% (Ahmad et al., 2016). PDMS-coated glassine wastepaper used in this study needed only 1.6% NaOCl to reach maximum crystallinity index of 78.90%. The concentration of NaOCl required for effective bleaching of cellulose is influenced by a variety of factors related to both the raw material and the processing conditions. The type of source material such as wood, agricultural residues or recycled paper, significantly impacts the necessary NaOCl concentration due to the differences in lignocellulosic composition and structure. Materials with higher lignin and hemicellulose content, typically require higher NaOCl concentrations for thorough bleaching. Additionally, the presence of impurities and the initial cellulose content also play important roles; materials with higher impurity levels often need more aggressive bleaching conditions.

3.4.3. Thermal analysis

Thermogravimetric analysis (TGA) was conducted to study the thermal behaviour of MCC by measuring mass loss in the samples as the temperature increased, enabling the quantification of material that decomposes over a particular temperature interval. The TGA and DTG profiles of extracted MCC at NaOCl ranging from 1.0% to 2.0% are reported in Fig. 8. The TGA curves reveal three distinct regions of weight loss, showing that all MCC samples experience similar major decomposition events. The initial weight loss at temperature below 100 °C is identified as the loss of free water and the release of bound water from the polymeric structure of MCC. The second region, between approximately 200-300 °C, is indicated by the initial significant drop in the weight loss curves. The third region, occurring between 300 and 400 °C, marked by a more substantial decrease in the curves. Beyond 400 °C, the weight loss stabilizes, indicating the completion of major decomposition process. This effect is more clearly illustrated in the differential thermogravimetry (DTG) curves, offering a comprehensive understanding of the thermal degradation behaviour of the MCC.

The DTG curve provide further insights into the decomposition behaviour, with peaks representing the temperatures at which the rate of weight loss is at its maximum (Libourel et al., 2020). The main DTG peak indicates cellulose degradation, with a shoulder at the lower temperature, signifying hemicellulose degradation. Hemicellulose, being less thermally stable than cellulose, decomposes at a slightly lower temperature, resulting in the shoulder observed in the DTG curve (Carrier et al., 2016; El-Gendy et al., 2020). The prominent crystalline peaks appearing around 328–333 °C in all MCC samples are typically indicative of high concentration of α-cellulose, which decomposes at higher temperature. Meanwhile the peak around 255 °C signifies the presence of a notable amount of hemicellulose. Variations in the TGA and DTG curves of MCC extracted at different NaOCl concentrations suggest subtle differences in

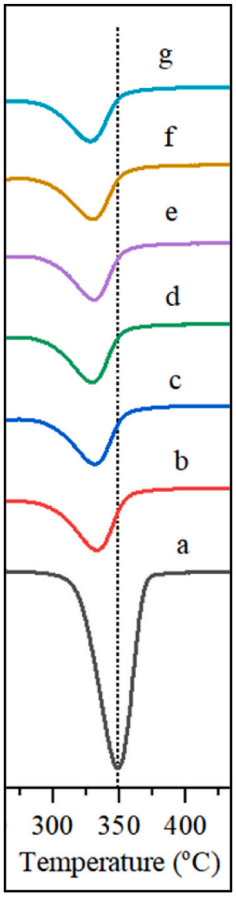

Fig. 9. Overlay of DTG curves of (a) commercial MCC and extracted MCC; (b) MCC1.0%, (c) MCC1.2%, (d) MCC1.4%, (e) MCC1.6%, (f) MCC1.8% and (g) MCC2.0%.

Table 2
TG/DTG data of MCC samples at T_{max} extracted at different NaOCl concentrations and commercial MCC.

Samples	Weight loss (%)	Rate of weight loss at T_{max} (%/s)	T_{onset} (°C)	T_{max} (°C)	T_{end} (°C)
MCC1.0%	44.26	−0.1406	274	333	373
MCC1.2%	43.63	−0.1434	273	332	372
MCC1.4%	43.57	−0.1407	273	331	369
MCC1.6%	43.26	−0.1445	272	331	369
MCC1.8%	41.65	−0.1341	271	331	368
MCC2.0%	40.10	−0.1340	269	328	367
Commercial MCC	88.48	−0.4544	293	350	375

thermal stability. The crystalline peak of extracted MCC had shifted to a lower temperature compared to commercial MCC and these interpretations and transitions can be seen clearly in Fig. 9. It was observed that as NaOCl concentration increases, the temperature of the crystalline peak at which decomposition occurs gradually decreases due to the progressive oxidation in the polymeric structure of cellulose. The oxidative process intensifies, leading to a more significant breakdown of the cellulose structure, which in turn causes it to decompose at lower temperature compared to commercial MCC and alter the thermal stability stability of MCC (Isogai et al., 2018).

Table 2 presents comprehensive TG/DTG data for MCC samples extracted with varying concentrations of NaOCl and commercial MCC as reference, highlighting the impact of NaOCl concentration on the thermal stability and decomposition behaviour of MCC. Specifically, it demonstrates the influence of NaOCl concentration on the temperature where the decomposition started, T_{onset}, maximum decomposition temperature, T_{max}, final decomposition temperature, T_{end}, and the weight loss at T_{max}. According to J. Wang et al. (2021), most hemicellulose and some amount of cellulose decomposed below the DTG shoulder temperature while the remaining cellulose degraded at higher temperature.

The onset and maximum decomposition temperature are vital indicators of a material's thermal stability. These properties provide valuable insights into how a material responds to thermal stress and are essential for evaluating its stability and performance in various

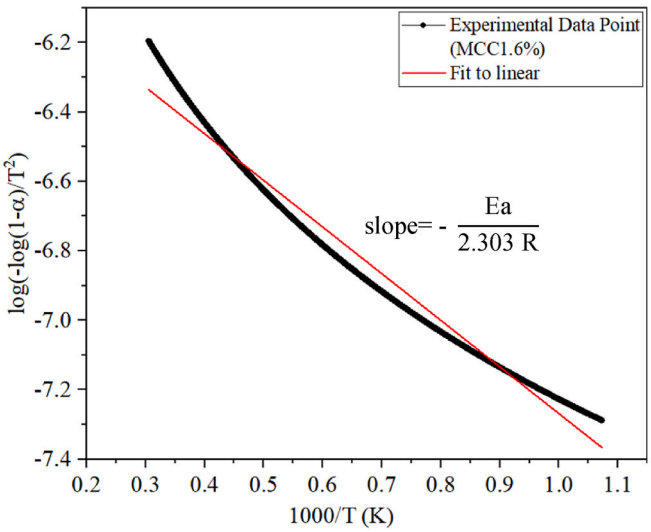

Samples	Activation energy, E_a ($kJmol^{-1}$)
MCC1.0%	25.682
MCC1.2%	25.676
MCC1.4%	25.678
MCC1.6%	25.688
MCC1.8%	25.669
MCC2.0%	25.683
Commercial MCC	22.842

Fig. 10. Coats and Redfern plot of extracted MCC to determine the activation energy (Ea).

applications. Analyzing the extraction process with lower NaOCl concentration, it is observed that these concentrations result in MCC with higher thermal degradation temperatures and greater weight loss. For example, the T_{max} for MCC extracted with 1.0% NaOCl is the highest at 333 °C with 44.26% weight loss. This suggests that the cellulose structure remains largely intact, retaining more of its original properties, which includes higher thermal stability and higher weight loss upon decomposition. As the NaOCl concentration increases to 2.0%, a slight decrease in T_{max} is observed. The T_{max} values decrease marginally to 328 °C for MCC2.0% with a notable decreasing trend in weight loss at T_{max}, of 40.10%. This small reduction in T_{max} indicates that higher concentrations of NaOCl may cause a slight degradation of the cellulose structure. The reduction of T_{max} where the temperature at which maximum decomposition occurs, indicates a decrease in thermal stability of a material to withstand at higher temperature without decomposing. In essence, the material becomes more prone to breaking down at lower temperatures, reflecting a compromised ability to resist thermal degradation. In this case, the reduction in thermal stability of MCC samples can be attributed to the modification of the cellulose structure induced by higher concentration of the oxidizing agent. The oxidative properties of NaOCl can break down the cellulose chains, rendering the chains more susceptible to thermal decomposition (Nakasone and Kobayashi, 2016). Oxidative modifications of cellulose structure by NaOCl can introduce functional groups such as carbonyl group and lead to the conversion to carboxyl group as the concentration of oxidant increases (Baron and Coseri, 2020). Even at a very low degree of carboxyl functionalization, the thermal stability is notably diminished compared to that of original cellulose (Sharma and Varma, 2014).

When the extraction is conducted at NaOCl concentration of 1.0%, the onset of degradation starts at a higher temperature of 274 °C and subsequently decreases to 269 °C as the concentration increases to 2.0%. Correspondingly, the weight loss progresses steadily, reaching T_{end} of 373 °C at the lowest concentration with weight loss rate, −0.1406 $\%s^{-1}$. At the highest concentration, there were only minor changes where the T_{end} decreasing slightly to 367 °C and a reduced weight loss rate of −0.1340 $\%s^{-1}$, indicating a minimal impact on the overall thermal decomposition process. Commercial MCC exhibits a significantly higher weight loss percentage of 88.48% and higher rate of weight loss at T_{max} of −0.4544 $\%s^{-1}$. In term of thermal stability, commercial MCC shows a superior performance where it started to decompose at higher temperature of 293 °C with a single step degradation curve. This indicates that high purity of commercial MCC can contribute to higher rate of degradation due to reduced interference from components like lignin, hemicellulose or other impurities (Erdal and Hakkarainen, 2022). The crystallinity of MCC may also influence the rate of weight loss. Degradation process of higher crystallinity cellulose is more abrupt and concentrated around the peak degradation temperature resulting in higher rate of weight loss at higher degradation temperature. According to Poletto et al. (2012), a higher number of hydrogen bonds between adjacent cellulose chains can result from a more densely packed cellulose structure. The increased hydrogen bonding contributes to a more orderly and crystalline arrangement within the cellulose, leading to greater overall crystallinity. Consequently, the enhanced crystallinity leads to improved thermal stability, as the ordered and tightly bonded structure requires more energy to break down. As conclusion, the TGA data corroborate the XRD results, demonstrating that as the concentration of NaOCl increases, the crystallinity of cellulose decreases, leading to a corresponding reduction in thermal stability (Leng et al., 2020; M. M. Rana & De la Hoz Siegler, 2023). Referring to T_{max} of MCC extracted with a NaOCl concentration of 1.6% which demonstrates the highest crystallinity among the MCC samples, commercial MCC exhibits higher thermal stability as evidenced by its higher Tmax of 342 °C in accordance to a study by Kerche et al. (2022).

The activation energy (E_a) required for the thermal decomposition of MCC was determined by analyzing the TGA data *via* the Coats-Redfern method (Coats and Redfern, 1965). This method is a widely utilized approach for studying the kinetics of thermal decomposition reactions, particularly under non-isothermal condition. For first-order reaction, the Coats-Redfern method provides the mathematical relation as outlined in Equation (6) (Kulkarni et al., 2019; Paswan et al., 2021).

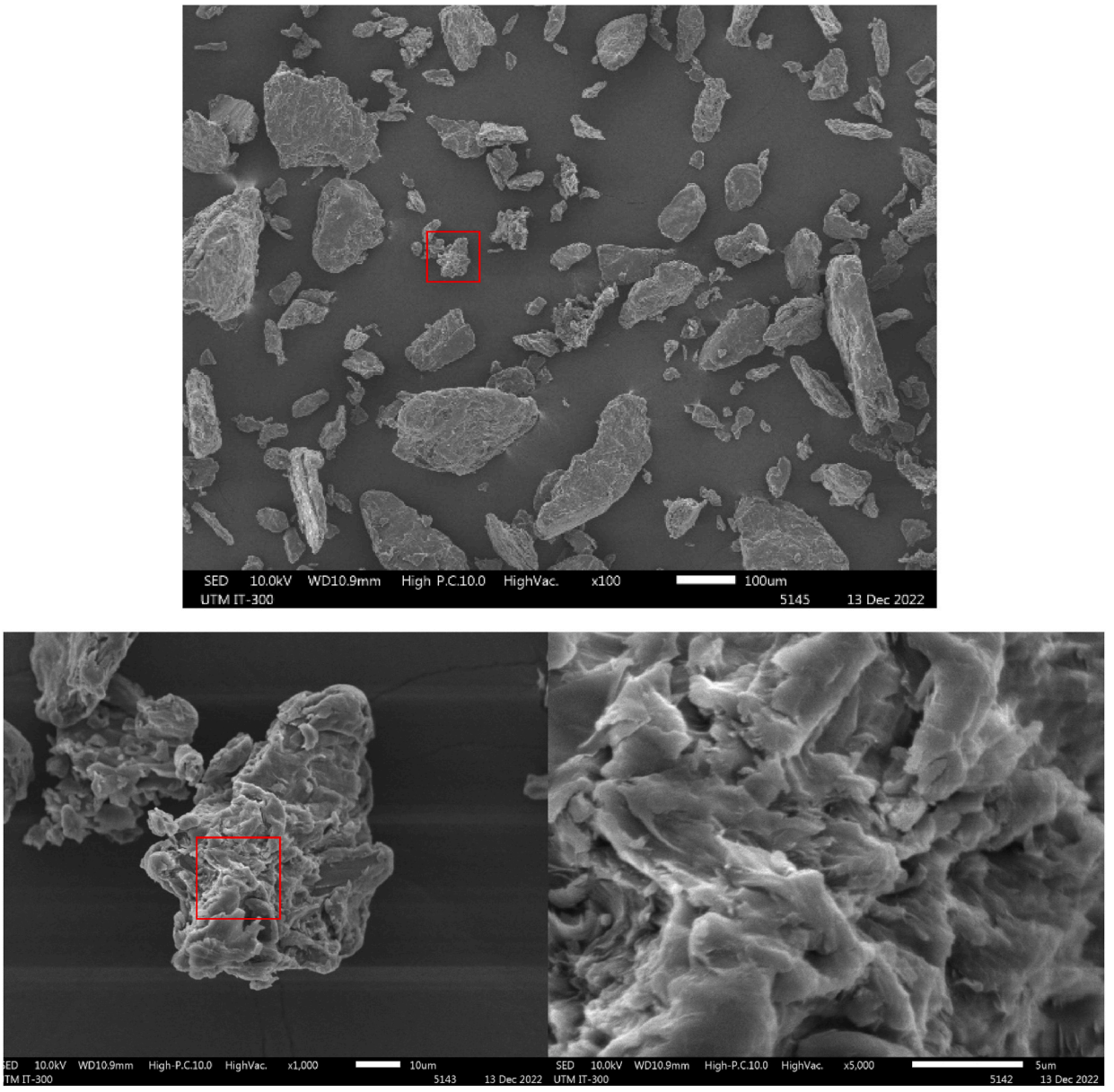

Fig. 11. Morphology of extracted MCC at different magnification of×100, ×1000 and x5000.

$$\log\left[\frac{-\log(1-\alpha)}{T^2}\right] = \log\frac{AR}{\beta E_a}\left[1-\frac{2RT}{E_a}\right] - \frac{E_a}{2.303RT} \quad \text{Equation 6}$$

In this context, α refer to the fraction of sample decomposed as defined in Equation (7):

$$\alpha = \frac{W_0 - W_t}{W_0 - W_f} \quad \text{Equation 7}$$

where W_t is the weight of sample at any given temperature T (mg), W_0 is the initial weight of the sample prior to decomposition reaction (mg), W_f is the final weight of the sample after the reaction is completed (mg); β is the heating rate (10 °C/min) and T is the absolute temperature (K).

In Fig. 10, a plot of $\log\left[\frac{-\log(1-\alpha)}{T^2}\right]$ against 1000/T is presented, where the term $\log\frac{AR}{\beta E_a}\left[1-\frac{2RT}{E_a}\right]$ is considered to be relatively constant for most values of E_a within the typical reaction temperature range. The linear relationship observed in the plot allows the determination of E_a, with the slope of the straight line corresponding to $\frac{E_a}{2.303R}$. According to Liang et al. (2023), the activation energy is

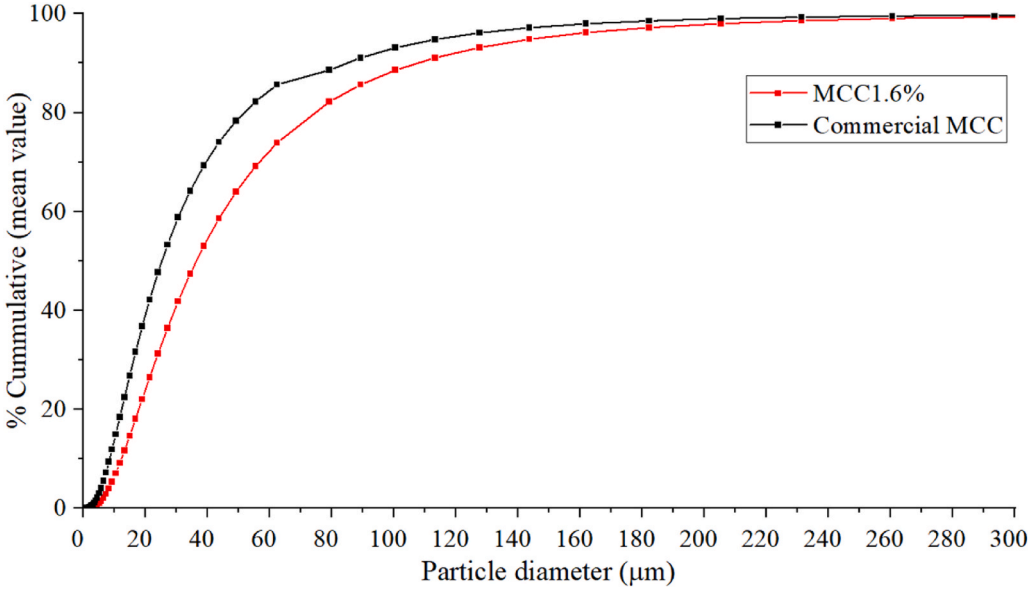

Fig. 12. Cumulative distribution of MCC1.6% and commercial MCC.

independent of the heating rate while thermal degradation is heating-rate dependent (Rantuch and Balog, 2014). The activation energy of all extracted MCC samples is found to be approximately 25 kJmol^{-1} which is marginally higher than that of commercial MCC, estimated at 22 kJmol^{-1}. The calculated activation energy for MCC derived from PDMS-coated glassine wastepaper aligns with previous studies where MCC from *Millettia pinnata* reported an activation energy of 25.349 kJmol^{-1} (Gopal P. M. et al., 2024) and MCC from *Lantana aculeata* leaves showed an activation energy of 30.12 kJmol^{-1} (Gokulkumar et al., 2023).

Notably, extracted cellulose demonstrate lower decomposition temperature at T_{max} coupled with higher activation energy compared to commercial MCC which exhibits the reverse thermal characteristics. This discrepancy may be attributed to residual remaining impurities in the extracted cellulose, potentially decreasing the decomposition temperature while increasing the activation energy (Guo et al., 2021).

3.4.4. Morphology and dimension analysis of MCC

The morphology of the extracted MCC sample was analyzed using SEM as depicted in Fig. 11. Following the successful removal of PDMS coating and non-cellulosic component during alkaline and bleaching treatment, coarse particles of different sizes were observed across all MCC samples. This variation in particle size is attributed to the effectiveness of the treatments in breaking down non-cellulosic material to leave behind the cellulosic part. The images reveal that despite varying concentrations, all MCC samples exhibit similar morphology and particle size. Moreover, the larger size of MCC particles may indicate a degree of aggregation, likely resulting from their lower solubility in water as noted by Alves et al. (2015). While some variations in texture and aggregation are observed, the overall morphology remains relatively consistent. Across the series from MCC1.0% to MCC2.0%, the particles consistently display similarity in size distribution. In conclusion, the SEM micrographs indicate that MCC samples, regardless of NaOCl concentration, maintain consistent particle morphology and size distribution. This consistency indicates that bleaching treatment using different NaOCl concentration during extraction do not substantially impact the fundamental structural characteristics of MCC. The MCC extracted from PDMS-coated glassine wastepaper, regardless of NaOCl concentrations used, feature higher aspect ratio, ranging from 1.9 to 2.3 whereas the commercial MCC shows an aspect ratio of 1.2–2.2. In the pharmaceutical industry, MCC particles with higher aspect ratio are often chosen to enhance the hardness of tablets. This is because the increased aspect ratio contributes to greater compressibility, allowing the particles to compact more tightly and create strong interparticle bonds (Horio et al., 2014).

To further investigate the particle size of MCC, MCC1.6% was selected as the optimal candidate for particle size analysis due to its comparable crystallinity with commercial MCC. Fig. 12 presents the cumulative distribution versus particle diameter of MCC1.6% and commercial MCC. The abbreviations; d_{10}, d_{50} and d_{90} refer to the particle sizes at which the cumulative size distribution reaches 10%, 50% and 90%, respectively. These values represent the particle sizes where d_{10} and d_{90} are critical in application when the presence of fine and course particles can affect the performance or quality of the material. For instance, in filtration processes, fine particles can lead to deposition within the internal structure of the medium while large particles tend to form a deposit on the medium's surface (Wakeman, 2007). The median diameter, d_{50}, represents the midpoint of the particle size distribution, where half of the particles are smaller and the other half are larger. This parameter is particularly important because it provides a central value that effectively summarizes the overall particle size distribution. It is observed that the d_{50} for MCC1.6% shows a larger average particle size of 36.4 μm compared to 28.5 μm for commercial MCC. Factors that contribute to the size differences of MCC are the source material and the chemical processing conditions (Das et al., 2010). For instance, MCC isolated from pistachio shells demonstrates smaller particles sizes

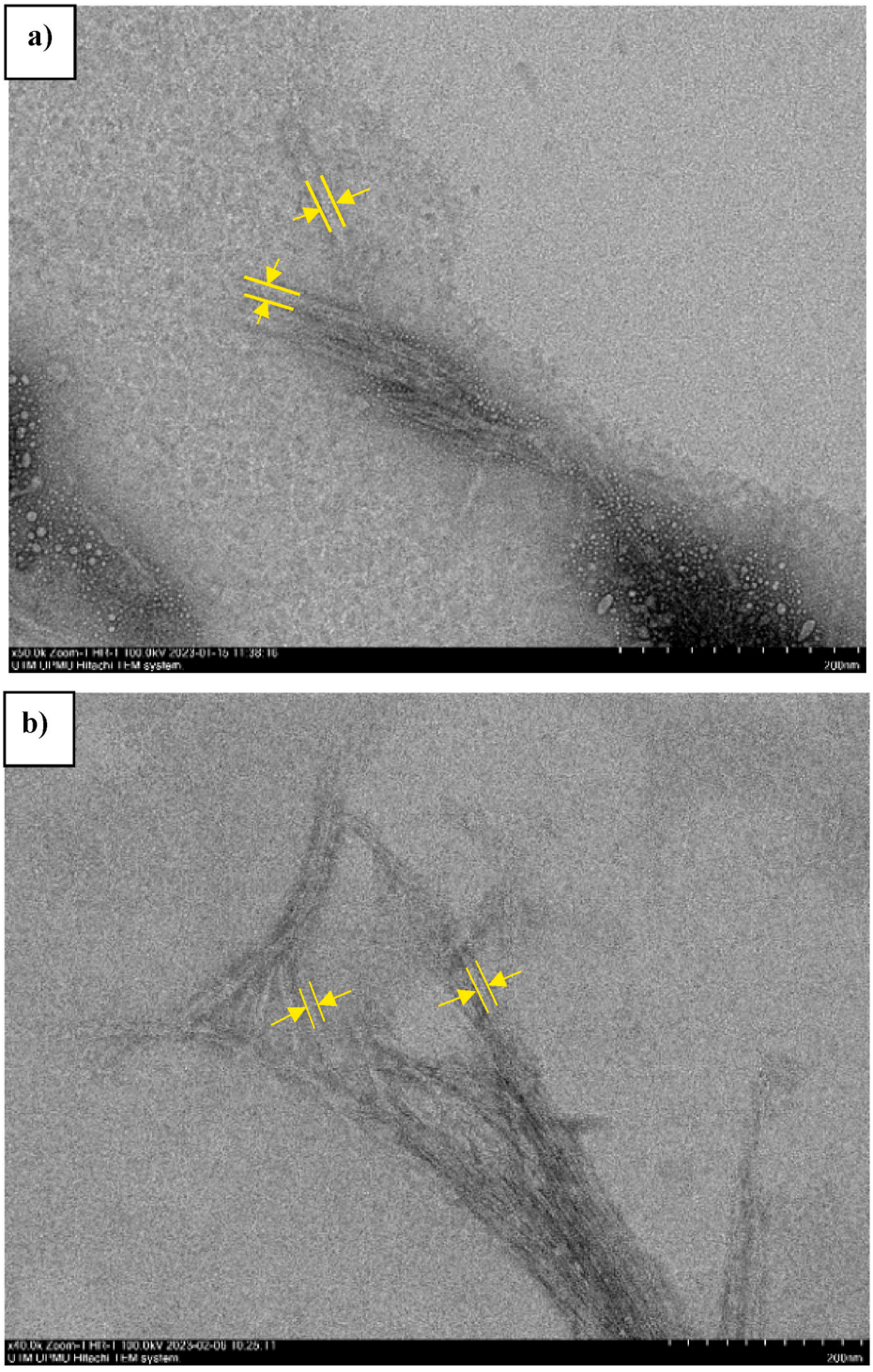

Fig. 13. High magnification TEM image of a) MCC1.6% and b) commercial MCC; yellow lines indicate the width of the microfibrils.

ranging from 21.47 nm to 29.40 nm, with a further decrease in size observed as the ratio of alkaline hydrogen peroxide (AHP) used to break down lignin increases (Park et al., 2010). In contrast, the particle size of MCC obtained from date seeds is considerably larger, falling in the range of 100–300 μm and is comparable to Avicel PH102 (100 μm) and Avicel PH200 (180 μm) (Abu-thabit et al., 2020)

The TEM images shown in Fig. 13 highlights a network of fibrous structures of MCC1.6% and commercial MCC samples. It was found that the cellulose fibers in MCC1.6% exhibit an average diameter of is 13.10 nm. This estimation was made by examining the

intertwined, elongated and tubular structure, marked by yellow lines in the image. Remarkably, this diameter is closely aligned with the fibrils observed in the commercial MCC, which have an average diameter of 12.80 nm. These findings indicate a significant similarity in the structural characteristics of MCC1.6% when compared to commercial MCC, suggesting that both materials share comparable physical properties. The fiber diameters observed in this study are also in agreement with those reported in previous research. For example, Abu-thabit et al. (2020) documented a fiber diameter of 13.61 nm for MCC obtained from date seeds while Owolabi et al. (2016) reported a diameter of 13.35 nm for MCC extracted from oil palm fronds.

4. Conclusion

The extraction of MCC from PDMS-coated wastepaper was effectively achieved through an alkaline treatment with NaOH followed by bleaching with NaOCl. In contrast to the conventional acid hydrolysis which is widely employed in MCC extraction from various substrates, this study presents an approach which eliminate the acid hydrolysis in MCC extraction. FTIR analysis confirmed the successful removal of the PDMS coating upon alkaline treatment, while the subsequent bleaching step exhibited a cellulosic spectral profile closely resembling that of commercial MCC. MCC extracted with 1.6% NaOCl concentration was found to have the highest CrI, of 78.90% with the smallest interplanar spacing (d_{002}) of 3.91 Å. However, the crystallinity showed a decline with increasing NaOCl concentration beyond 1.6% due to intensified oxidative bleaching. The thermal analysis of extracted MCC samples shows a decomposition temperature range between 328 and 333 °C and activation energy of approximately 25.6 kJmol^{-1}. Morphological analysis revealed a rough and irregular shape with aspect ratio and particle size slightly higher than that of commercial MCC. Notably, MCC from PDMS-coated wastepaper extracted using 5% NaOH and 1.6% NaOCl demonstrated comparable properties to commercial MCC, offering a viable alternative to acid hydrolysis under optimal treatment conditions.

CRediT authorship contribution statement

Nuhairi Alias: Writing – review & editing, Writing – original draft, Visualization, Methodology, Investigation, Formal analysis, Data curation, Conceptualization. **Che Rozid Mamat:** Visualization, Validation, Supervision, Conceptualization. **Zaiton Abdul Majid:** Validation, Supervision, Project administration, Funding acquisition. **Nur Faraliana Japri:** Resources. **Nur Hafizah A. Khalid:** Funding acquisition.

Declaration of competing interest

The authors declare the following financial interests/personal relationships which may be considered as potential competing interests:

Zaiton Abdul Majid reports financial support was provided by Ministry of Higher Education, Malaysia. Nur Hafizah Abd Khalid reports financial support was provided by Universitas Sriwijaya, Indonesia. If there are other authors, they declare that they have no known competing financial interests or personal relationships that could have appeared to influence the work reported in this paper.

Acknowledgement

The authors would like to acknowledge the technical and financial support from Ministry of Higher Education, Malaysia under Fundamental Research Grant Scheme (FRGS/1/2019/STG01/UTM/02/6) and Universitas Sriwijaya, Indonesia (R. J130000.7351.4525).

Data availability

Data will be made available on request.

References

Abolore, R.S., Jaiswal, S., Jaiswal, A.K., 2024. Green and sustainable pretreatment methods for cellulose extraction from lignocellulosic biomass and its applications: a review. Carbohydrate Polymer Technologies and Applications 7 (November 2023), 100396–100423. https://doi.org/10.1016/j.carpta.2023.100396.

Abu-thabit, N.Y., Abu, A., Hakeem, A.S., Ul-hamid, A., Umar, Y., Ahmad, A., 2020. Isolation and characterization of microcrystalline cellulose from date seeds (Phoenix dactylifera L.). Int. J. Biol. Macromol. 155, 730–739. https://doi.org/10.1016/j.ijbiomac.2020.03.255.

Adawiyah, R., Suryanti, V., Pranoto, 2022. Preparation and characterization of microcrystalline cellulose from lembang (Typha angustifolia L.). J. Phys. Conf. 2190 (1), 1–12. https://doi.org/10.1088/1742-6596/2190/1/012007.

Agboeze, E., Theresa O, U., Ogbobe, O., 2022. Extraction and characterization of pharmaceutical grade microcrystalline cellulose from Raphia Farinifera inflorescence. Universal Journal of Pharmaceutical Research 7 (4), 59–67. https://doi.org/10.22270/ujpr.v7i4.816.

Ahmad, Z., Roziaizan, N.N., Rahman, R., Mohamad, A.F., Wan Ismail, W.I.N., 2016. Isolation and characterization of microcrystalline cellulose (MCC) from rice husk (RH). MATEC Web of Conferences 47 (5013), 7. https://doi.org/10.1051/matecconf/20164705013.

Ahvenainen, P., Kontro, I., Svedström, K., 2016. Comparison of sample crystallinity determination methods by X-ray diffraction for challenging cellulose I materials. Cellulose 23 (2), 1073–1086. https://doi.org/10.1007/s10570-016-0881-6.

Akram Khan, M., Guru, S., Padmakaran, P., Mishra, D., Mudgal, M., Dhakad, S., 2011. Characterisation studies and impact of chemical treatment on mechanical properties of sisal fiber. Compos. Interfac. 18 (6), 527–541. https://doi.org/10.1163/156855411X610250.

Alves, L., Medronho, B., Antunes, F.E., Fernández-García, M.P., Ventura, J., Araújo, J.P., Romano, A., Lindman, B., 2015. Unusual extraction and characterization of nanocrystalline cellulose from cellulose derivatives. J. Mol. Liq. 210 (October 2015), 106–112. https://doi.org/10.1016/j.molliq.2014.12.010.

Ansharullah, A., Asniarb, A., Nurdinc, M., Saenuddin, N.M.A., Faradilla, R.F., Asranudin, A., 2020. Production of micro crystalline cellulose from tapioca solid waste: effect of acid concentration on its physico-chemical properties. Jurnal Kimia Sains Dan Aplikasi 23 (5), 147–151. https://doi.org/10.14710/jksa.23.5.147-151.
Aridi, A.S., Chin, N.L., Ishak, N.A., Mohamad Yusof, N.N., Kadota, K., Manaf, Y.N., Yusof, Y.A., 2021. Effect of sodium hypochlorite concentration during pre-treatment on isolation of nanocrystalline cellulose from Leucaena leucocephala (Lam.) mature pods. Bioresources 16 (2), 3137–3158. https://doi.org/10.15376/biores.16.2.3137-3158.
Arnata, I.W., Suprihatin, S., Fahma, F., Richana, N., Candra Sunarti, T., 2019. Cellulose production from sago frond with alkaline delignification and bleaching on various types of bleach agents. Orient. J. Chem. 35 (Special Issue 1), 8–19. https://doi.org/10.13005/ojc/35Specialissue102.
Aurelia, C., Murdiati, A., Supriyanto, Ningrum, A., 2019. Effect of sodium hydroxide and sodium hypochlorite on the physicochemical characteristics of jack bean skin (Canavalia ensiformis). Pakistan J. Nutr. 18 (2), 193–200. https://doi.org/10.3923/pjn.2019.193.200.
Backere, C. de, Quodbach, J., Beer, T. De, Vervaet, C., Vanhoorne, V., 2022. Impact of alternative lubricants on process and tablet quality for direct compression. Int. J. Pharm. 624 (May), 1–13. https://doi.org/10.1016/j.ijpharm.2022.122012.
Bali, G., Meng, X., Deneff, J.I., Sun, Q., Ragauskas, A.J., 2015. The effect of alkaline pretreatment methods on cellulose structure and accessibility in milled Populus. ChemSusChem 8 (2), 275–279. https://doi.org/10.1002/cssc.201402752.
Barman, D.N., Haque, M.A., Hossain, M.M., Paul, S.K., Yun, H.D., 2020. Deconstruction of pine wood (Pinus sylvestris) recalcitrant structure using alkali treatment for enhancing enzymatic saccharifcation evaluated by Congo Red. Waste and Biomass Valorization 11 (5), 1755–1764. https://doi.org/10.1007/s12649-018-00547-z.
Baron, R.I., Coseri, S., 2020. Preparation of water-soluble cellulose derivatives using TEMPO radical-mediated oxidation at extended reaction time. React. Funct. Polym. 157 (June), 1–10. https://doi.org/10.1016/j.reactfunctpolym.2020.104768.
Budtova, T., Navard, P., 2016. Cellulose in NaOH–water based solvents: a review. Cellulose 23 (1), 1–105. https://doi.org/10.1007/s10570-015-0779-8.
Carrier, M., Auret, L., Bridgwater, A., Knoetze, J.H., 2016. Using apparent activation energy as a reactivity criterion for biomass pyrolysis. Energy & Fuels 30 (10), 7834–7841. https://doi.org/10.1021/acs.energyfuels.6b00794.
Çavdar, A.D., Yel, H., Torun, S.B., 2022. Microcrystalline cellulose addition effects on the properties of wood cement boards. J. Build. Eng. 48 (December 2021), 1–9. https://doi.org/10.1016/j.jobe.2021.103975.
Cerro, D. R. del, Koso, T.V., Kakko, T., King, A.W.T., Kilpelainen, I., 2020. Crystallinity reduction and enhancement in the chemical reactivity of cellulose by non-dissolving pre-treatment with tetrabutylphosphonium acetate. Cellulose 27 (10), 5545–5562. https://doi.org/10.1007/s10570-020-03044-6.
Chen, Q., Endo, T., Wang, Q., 2016. Characterization of microcrystalline cellulose after pretreatment with low concentrations of ionic liquid- H2O for a pyrolysis process. Bioresources 11, 159–173.
Cichosz, S., Masek, A., 2020. IR study on cellulose with the varied moisture contents: insight into the supramolecular structure. Materials 13 (4573), 1–22. https://doi.org/10.3390/ma13204573.
Coats, A.W., Redfern, J.P., 1965. Kinetic parameters from thermogravimetric data. Polymer Letters 3, 917–920.
Cui, T., Li, J., Yan, Z., Yu, M., Li, S., 2014. The correlation between the enzymatic saccharification and the multidimensional structure of cellulose changed by different pretreatments. Biotechnol. Biofuels 7 (1), 1–10. https://doi.org/10.1186/s13068-014-0134-6.
Das, K., Ray, D., Bandyopadhyay, N.R., Sengupta, S., 2010. Study of the properties of microcrystalline cellulose particles from different renewable resources by XRD, FTIR, nanoindentation, TGA and SEM. J. Polym. Environ. 18 (3), 355–363. https://doi.org/10.1007/s10924-010-0167-2.
Deshwal, G.K., Panjagari, N.R., Alam, T., 2019. An overview of paper and paper based food packaging materials: health safety and environmental concerns. J. Food Sci. Technol. 56 (10), 4391–4403. https://doi.org/10.1007/s13197-019-03950-z.
Egamberdiev, E.A., Norboyev, S.K., 2022. Extraction of cellulose nanocrystals from secondary paper waste and their use in paper production. Technical Science and Innovation 2022 (3), 12. https://doi.org/10.51346/tstu-01.22.3-77-0195.
El-Gendy, A., El-Sakhawy, M., Adel, A.M., Al-Shemy, M.T., 2020. Effect of microcrystalline cellulose as a filler and/or filler retention aid on the mechanical properties of bagasse paper sheets. Cellul. Chem. Technol. 54 (9–10), 993–1000. https://doi.org/10.35812/cellulosechemtechnol.2020.54.96.
Erdal, N.B., Hakkarainen, M., 2022. Degradation of cellulose derivatives in laboratory, man-made, and natural environments. Biomacromolecules 23 (7), 2713–2729. https://doi.org/10.1021/acs.biomac.2c00336.
Esteves, C.V.G., Sevastyanova, O., Östlund, S., Brännvall, E., 2022. The impact of bleaching on the yield of softwood kraft pulps obtained by high alkali impregnation. Nord. Pulp Pap Res. J. 37 (4), 593–608. https://doi.org/10.1515/npprj-2022-0035.
Estrela, C., Estrela, C.R.A., Barbin, E.L., Spanó, J.C.E., Marchesan, M.A., Pécora, J.D., 2002. Mechanism of action of sodium hypochlorite. Braz. Dent. J. 13 (2), 113–117. https://doi.org/10.1590/S0103-64402002000200007.
Flórez-Pardo, L.M., González-Córdoba, A., López-Galán, J.E., 2019. Characterization of hemicelluloses from leaves and tops of the CC 8475, CC 8592, and V 7151 varieties of sugarcane (Saccharum officinarum l.). Dyna 86 (210), 98–107. https://doi.org/10.15446/dyna.v86n210.75757.
Fu, J., Yang, F., Cheng, F., Guo, Z., 2022. Preparation of an electrically conductive, flame-retardant, and superhydrophobic recycled paper. Colloids Surf. A Physicochem. Eng. Asp. 642 (December 2021), 1–7. https://doi.org/10.1016/j.colsurfa.2022.128671.
Garrido, L.H., Schnitzler, E., Zortéa, M.E.B., de Souza Rocha, T., Demiate, I.M., 2014. Physicochemical properties of cassava starch oxidized by sodium hypochlorite. J. Food Sci. Technol. 51 (10), 2640–2647. https://doi.org/10.1007/s13197-012-0794-9.
Gaudreault, R., Van De Ven, T.G.M., Whitehead, M.A., 2005. Mechanisms of flocculation with poly(ethylene oxide) and novel cofactors. Colloids Surf. A Physicochem. Eng. Asp. 268 (1–3), 131–146. https://doi.org/10.1016/j.colsurfa.2005.04.044.
Gokulkumar, S., Suyambulingam, I., Divakaran, D., Priyadharshini, G.S., Aravindh, M., Iyyadurai, J., Edwards, M.S., Siengchin, S., 2023. Facile exfoliation and physicochemical characterization of biomass-based cellulose derived from Lantana aculeata leaves for sustainable environment. Macromol. Res. 31 (12), 1163–1178. https://doi.org/10.1007/s13233-023-00197-8.
Gopal, P.M., Suganya Priyadharshini, G., Suyambulingam, I., Divakaran, D., Kavimani, V., Sanjay, M.R., Siengchin, S., 2024. Exfoliation and physicochemical characterization of novel biomass-based microcrystalline cellulose derived from Millettia pinnata leaf. Biomass Conversion and Biorefinery 14 (17), 20189–20199. https://doi.org/10.1007/s13399-023-04059-2.
Gordon, G., Adam, L.C., Bubnis, B.P., Kuo, C., Cushing, R.S., Sakaji, R.H., 1997. Predicting liquid bleach decomposition. American Water Works Association 89 (4), 142–149.
Guo, W., Li, Y., Xiao, W., Li, J., Han, Z., Wang, B., 2021. Mechanism of two typical binders BR and F2604 on thermal decomposition of HMX. ACS Omega 6 (3), 2025–2033. https://doi.org/10.1021/acsomega.0c04985.
Hafid, H.S., Omar, F.N., Bahrin, E.K., Wakisaka, M., 2023. Extraction and surface modification of cellulose fibers and its reinforcement in starch-based film for packaging composites. Bioresources and Bioprocessing 10 (1), 7. https://doi.org/10.1186/s40643-023-00631-w.
Han, J.S., Jung, S.Y., Kang, D.S., Seo, Y.B., 2020. Development of flexible calcium carbonate for papermaking filler. ACS Sustain. Chem. Eng. 8 (24). https://doi.org/10.1021/acssuschemeng.0c01593.
Haryanti, N.H., Suryajaya, Suarso, Khaipanurani, E., Manik, T.N., 2022. Modification of purun tikus (Eleocharis dulcis) long fiber with potential as composite reinforcement material. J. Phys. Conf. 2392 (1). https://doi.org/10.1088/1742-6596/2392/1/012031.
Hong, T., Yin, J.-Y., Nie, S.-P., Xie, M.-Y., 2021. Applications of infrared spectroscopy in polysaccharide structural analysis: progress, challenge and perspective. Food Chem. X 12 (October), 1–16. https://doi.org/10.1016/j.fochx.2021.100168.
Horio, T., Yasuda, M., Matsusaka, S., 2014. Effect of particle shape on powder flowability of microcrystalline cellulose as determined using the vibration shear tube method. Int. J. Pharm. 473 (1–2), 572–578. https://doi.org/10.1016/j.ijpharm.2014.07.040.
Hosseinzadeh, J., Abdulkhani, A., Ashori, A., Dmirievich, P.S., Abdolmaleki, H., Hajiahmad, A., Sun, F., Zadeh, Z.E., 2024. Comparative study on liquid versus gas phase hydrochloric acid hydrolysis for microcrystalline cellulose isolation from sugarcane bagasse. Int. J. Biol. Macromol. 264 (P2), 130674. https://doi.org/10.1016/j.ijbiomac.2024.130674.
Howell, C., Hastrup, A.C.S., Jara, R., Larsen, F.H., Goodell, B., Jellison, J., 2011. Effects of hot water extraction and fungal decay on wood crystalline cellulose structure. Cellulose 18 (5), 1179–1190. https://doi.org/10.1007/s10570-011-9569-0.

Huang, H., Zhang, Y., Liu, Y., Guo, Y., Hu, C., 2023. Influence of intermolecular interactions on crystallite size in crystalline solid dispersions. Pharmaceutics 15 (10), 2493. https://doi.org/10.3390/pharmaceutics15102493.
Isogai, A., Hänninen, T., Fujisawa, S., Saito, T., 2018. Review: catalytic oxidation of cellulose with nitroxyl radicals under aqueous conditions. Prog. Polym. Sci. 86, 122–148. https://doi.org/10.1016/j.progpolymsci.2018.07.007.
Isroi, Cifriadi, A., Panji, T., Wibowo, N.A., Syamsu, K., 2017. Bioplastic production from cellulose of oil palm empty fruit bunch. IOP Conf. Ser. Earth Environ. Sci. 65. https://doi.org/10.1088/1755-1315/65/1/012011.
Isroi, I., Cifriadi, A., 2018. Oxidation of cellulose from oil palm empty fruit bunch using hydrogen peroxide in alkaline condition. Jurnal Selulosa 8 (2), 51–60. https://doi.org/10.25269/jsel.v8i02.233.
Iwamiya, Y., Nishio-Hamane, D., Akutsu-Suyama, K., Arima-Osonoi, H., Shibayama, M., Hiroi, Z., 2022. Photocatalytic silica–resin coating for environmental protection of paper as a plastic substitute. Ind. Eng. Chem. Res. 61 (20), 6967–6972. https://doi.org/10.1021/acs.iecr.2c00784.
Janmohammadi, M., Nazemi, Z., Salehi, A.O.M., Seyfoori, A., John, J.V., Nourbakhsh, M.S., Akbari, M., 2023. Cellulose-based composite scaffolds for bone tissue engineering and localized drug delivery. Bioact. Mater. 20 (February 2022), 137–163. https://doi.org/10.1016/j.bioactmat.2022.05.018.
Johnson, L.M., Gao, L., IV, C.W.S., Smith, M., Efimenko, K., Cushing, K., Genzer, J., López, G.P., 2013. Elastomeric microparticles for acoustic mediated bioseparations. J. Nanobiotechnol. 11 (1), 22. https://doi.org/10.1186/1477-3155-11-22.
Junadi, N., Beg, M.D.H., Yunus, R.M., Ramli, R., Azrina, Z.A.Z., Alam, A.K.M.M., 2019. Characterization of microcrystalline cellulose isolated through mechanochemical method. Indian J. Fibre Text. Res. 44 (December), 442–449. https://doi.org/10.56042/ijftr.v44i4.19886.
Junior, C.S., Milagres, A.M.F., Ferraz, A., Carvalho, W., 2013. The effects of lignin removal and drying on the porosity and enzymatic hydrolysis of sugarcane bagasse. Cellulose 20 (6), 3165–3177. https://doi.org/10.1007/s10570-013-0032-2.
Kaden, W.E., Pomp, S., Sterrer, M., Freund, H.-J., 2017. Insights into silica bilayer hydroxylation and dissolution. Top. Catal. 60 (6–7), 471–480. https://doi.org/10.1007/s11244-016-0715-7.
Karlson, K.R., 1951. Manufacture of glassine paper. In: United States Patent Office.
Kaza, S., Yao, L., Bhada-Tata, P., Woerden, F. Van, 2018. What a Waste 2.0: A Global Snapshot of Solid Waste Management to 2050. World Bank Publications. https://doi.org/10.1596/978-1-4648-1329-0.
Kerche, E.F., Neves, R.M., Ornaghi, H.L., Zattera, A.J., Schrekker, H.S., 2022. The influence of ionic liquid concentration on microcrystalline cellulose modification. Carbohydrate Polymer Technologies and Applications 3 (May), 100211. https://doi.org/10.1016/j.carpta.2022.100211.
Khoshsepehr, Z., Alinejad, S., Alimohammadlou, M., 2023. Exploring industrial waste management challenges and smart solutions: an integrated hesitant fuzzy multi-criteria decision-making approach. J. Clean. Prod. 420 (August), 1–23. https://doi.org/10.1016/j.jclepro.2023.138327.
Kostryukov, S.G., Matyakubov, H.B., Masterova, Y.Y., Kozlov, A.S., Pryanichnikova, M.K., Pynenkov, A.A., Khluchina, N.A., 2023. Determination of lignin, cellulose, and hemicellulose in plant materials by FTIR spectroscopy. J. Anal. Chem. 78 (6), 718–727. https://doi.org/10.1134/S1061934823040093.
Krumpfer, J.W., McCarthy, T.J., 2011. Rediscovering silicones: “unreactive” silicones react with inorganic surfaces. Langmuir 27 (18), 11514–11519. https://doi.org/10.1021/la202583w.
Kulkarni, A.B., Mathad, S.N., Bakale, R.P., 2019. The evaluation of kinetic parameters for cadmium doped Co-Zn ferrite using thermogravimetric analysis. Sciendo 30 (1), 60–64. https://doi.org/10.2478/auoc-2019-0011.
Lei, W., Fang, C., Zhou, X., Yin, Q., Pan, S., Yang, R., Liu, D., Ouyang, Y., 2018. Cellulose nanocrystals obtained from office waste paper and their potential application in PET packing materials. Carbohydr. Polym. 181 (October 2017), 376–385. https://doi.org/10.1016/j.carbpol.2017.10.059.
Lei, W., Zhou, X., Fang, C., Li, Y., Song, Y., Wang, C., Huang, Z., 2019. New approach to recycle office waste paper : reinforcement for polyurethane with nano cellulose crystals extracted from waste paper. Waste Manag. 95, 59–69. https://doi.org/10.1016/j.wasman.2019.06.003.
Leng, E., Ferreiro, A.I., Liu, T., Gong, X., Costa, M., Li, X., Xu, M., 2020. Experimental and kinetic modelling investigation on the effects of crystallinity on cellulose pyrolysis. J. Anal. Appl. Pyrol. 152 (May), 104863. https://doi.org/10.1016/j.jaap.2020.104863.
Lenkiewicz, Z., Bernardes, F., Halpaap, A., Louzada, L., Ramola, A., Filho, C.S., Souza, H.H.S., Smith, J., Ternald, D., Wilson, D., Smith, J., 2024. Beyond an Age of Waste.
Li, W., Wang, Y., Liu, R., Chen, W., Zhang, H., Zhang, Z., 2023. Gel polymer-based composite solid-state electrolyte for long-cycle-life rechargeable zinc–air batteries. ACS Sustain. Chem. Eng. 11 (9), 3732–3739. https://doi.org/10.1021/acssuschemeng.2c06661.
Liang, Y., Ries, M.E., Hine, P.J., 2023. Pyrolysis activation energy of cellulosic fibres investigated by a method derived from the first order global model. Carbohydr. Polym. 305, 1–10. https://doi.org/10.1016/j.carbpol.2022.120518.
Libourel, G., Ganino, C., Delbo, M., Niezgoda, M., Remy, B., Aranda, L., Michel, P., 2020. Network of thermal cracks in meteorites due to temperature variations: new experimental evidence and implications for asteroid surfaces. Mon. Not. Roy. Astron. Soc. 500 (2), 1905–1920. https://doi.org/10.1093/mnras/staa3183.
Mhike, W., Dewa, L., Tichapondwa, S.M., 2023. Adsorption of hexavalent chromium from wastewater using microcrystalline cellulose. Chemical Engineering Transactions 103 (April), 661–666. https://doi.org/10.3303/CET23103111.
Modenbach, A.A., Nokes, S.E., 2014. Effects of sodium hydroxide pretreatment on structural components of biomass. Transactions of the ASABE 57 (4), 1187–1198. https://doi.org/10.13031/trans.57.10046.
Mohammed Irfan, T.N., Sunitha George, T., Sainul Abidh, K.M., Prakash, S., Parambath Kanoth, B., George, N., Balachandrakurup, V., Midhun Dominic, C.D., Nair, A. B., 2023. Waste paper as a viable sustainable source for cellulosic extraction by chlorine free bleaching and acid hydrolysis method for the production of PVA-starch/cellulose based biocomposites. Mater. Today: Proc. https://doi.org/10.1016/j.matpr.2023.03.805.
Nakasone, K., Kobayashi, T., 2016. Effect of pre-treatment of sugarcane bagasse on the cellulose solution and application for the cellulose hydrogel films. Polym. Adv. Technol. https://doi.org/10.1002/pat.3757. December 2015.
Ni’mah, H., Ningrum, E.O., Sumarno, Rizkiyah, D.N., Divta, I.G.A.G.C., Meiliefiana, Subaghio, M.A., 2017. Effect of particle size and crystallinity of cellulose filler on the properties of poly(L-lactic acid): mechanical property and thermal stability. AIP Conf. Proc. 1840 (February 2021). https://doi.org/10.1063/1.4982317, 090009-1-090009–2.
Nsor-Atindana, J., Chen, M., Goff, H.D., Zhong, F., Sharif, H.R., Li, Y., 2017. Functionality and nutritional aspects of microcrystalline cellulose in food. Carbohydr. Polym. 172, 159–174. https://doi.org/10.1016/j.carbpol.2017.04.021.
Nur Hanani, A.S., Zuliahani, A., Nawawi, W.I., Razif, N., Rozyanty, A.R., 2017. The effect of various acids on properties of microcrystalline cellulose (MCC) extracted from rice husk (RH). IOP Conf. Ser. Mater. Sci. Eng. 204 (1), 1–6. https://doi.org/10.1088/1757-899X/204/1/012025.
Örn, A., 2019. Degradation Studies on Polydimethylsiloxane (Issue May).
Owolabi, A.F., Ghazali, A., Khalil, H.P.S.A., Hassan, A., Arjmandi, R., Fazita, M.R.N., Haafiz, M.K.M., 2016. Isolation and characterization of microcrystalline cellulose from oil palm fronds using chemomechanical process. Wood Fiber Sci. 48 (4), 260–270.
Park, So-yoon, Kim, H., Her, J., 2024. Isolation of microcrystalline cellulose (MCC) from pistachio shells and preparation of carrageenan-based composite films. Carbohydrate Polymer Technologies and Applications 7 (January), 1–12. https://doi.org/10.1016/j.carpta.2024.100423.
Park, Sunkyu, Baker, J.O., Himmel, M.E., Parilla, P.A., Johnson, D.K., 2010. Cellulose crystallinity index: measurement techniques and their impact on interpreting cellulase performance. Biotechnol. Biofuels 3 (1), 10. https://doi.org/10.1186/1754-6834-3-10.
Peleg, M., 2023. On modeling the temperature effects on biopolymers and foods undergoing glass transition without the WLF equation. Food Engineering Reviews 15, 381–392.
Poletto, M., Júnior, H.L.O., Zattera, A.J., 2014. Native cellulose: structure, characterization and thermal properties. Materials 7, 6105–6119. https://doi.org/10.3390/ma7096105.
Poletto, M., Zattera, A.J., Forte, M.M.C., Santana, R.M.C., 2012. Thermal decomposition of wood: influence of wood components and cellulose crystallite size. Bioresour. Technol. 109, 148–153. https://doi.org/10.1016/j.biortech.2011.11.122.
Polettoa, M., Pistorc, V., Santanaa, R.M.C., Zattera, A.J., 2012. Materials produced from plant biomass . Part II : evaluation of crystallinity and degradation kinetics of cellulose. Mater. Res. 15 (3), 421–427. https://doi.org/10.1590/S1516-14392012005000048.

Poyraz, B., Tozluoğlu, A., Candan, Z., Demir, A., Yavuz, M., Büyuksarı, Ü., Ünal, H.İ., Fidan, H., Saka, R.C., 2018. TEMPO-treated CNF composites: pulp and matrix effect. Fibers Polym. 19 (1), 195–204. https://doi.org/10.1007/s12221-018-7673-y.
Qin, H., Ma, C., Gärtner, S., Headen, T.F., Zuo, T., Jiao, G., Han, Z., Imberti, S., Han, C.C., Cheng, H., 2021. Neutron total scattering investigation on the dissolution mechanism of trehalose in NaOH/urea aqueous solution. Structural Dynamics 8 (1), 1–8. https://doi.org/10.1063/4.0000065.
Rana, M.M., De la Hoz Siegler, H., 2023. Influence of ionic liquid (IL) treatment conditions in the regeneration of cellulose with different crystallinity. J. Mater. Res. 38 (2), 328–336. https://doi.org/10.1557/s43578-022-00797-7.
Rana, R.H., Rana, M.S., Tasnim, S., Haque, M.R., Kabir, S., Amran, M.S., Chowdhury, A.A., 2022. Characterization and tableting properties of microcrystalline cellulose derived from waste paper via hydrothermal method. J. Appl. Pharmaceut. Sci. 12 (6), 140–147. https://doi.org/10.7324/JAPS.2022.120613.
Rantuch, P., Balog, K., 2014. Thermogravimetric analysis of cellulose insulation and determination of activation energy of its thermo-oxidation using non-isothermal, model-free methods. Polym. Adv. Technol. 25 (10), 1169–1174. https://doi.org/10.1002/pat.3373.
Ren, W., Zhu, J., Guo, F., Guo, J., Zhang, X., Wang, H., Yu, Y., 2022. Structural evolution of cellulose from bamboo fibers and parenchyma Cells during ionic liquid pretreatment for enhanced hydrolysis. Biomacromolecules 23 (5), 1938–1948. https://doi.org/10.1021/acs.biomac.1c01521.
Riseh, R.S., Vazvani, M.G., Hassanisaadi, M., Thakur, V.K., 2024. Agricultural wastes: a practical and potential source for the isolation and preparation of cellulose and application in agriculture and different industries. Ind. Crop. Prod. 208 (November 2023), 1–6. https://doi.org/10.1016/j.indcrop.2023.117904.
Rodrigues, P. de O., Correa, A.G., Baffi, M.A., Pasquini, D., 2023. In: Thomas, S., Hosur, M., Pasquini, D., Jose Chirayil, C. (Eds.), Potential Applications of Hemicellulose. Springer Nature Singapore, Issue December. https://doi.org/10.1007/978-981-19-6772-6.
Salem, K.S., Kasera, N.K., Rahman, M.A., Jameel, H., Habibi, Y., Eichhorn, S.J., French, A.D., Pal, L., Lucia, L.A., 2023. Comparison and assessment of methods for cellulose crystallinity determination. Chem. Soc. Rev. 52 (18), 6417–6446. https://doi.org/10.1039/d2cs00569g.
Salem, W., Us, N.C., Mark, S., Dooly, L., Us, N.C., Gerardi, A.R., Us, N.C., Neil, D., 2016. Method for Producing Microcrystalline Cellulose from Tobacco and Related Tobacco Product.
Samyn, P., Driessen, F., Stanssens, D., 2020. Natural rubber composites for paper coating applications. 2nd Coatings and Interfaces Web Conference (CIWC-2 2020) 29. https://doi.org/10.3390/CIWC2020-06832. May.
Sang, X., Qin, C., Tong, Z., Kong, S., Jia, Z., Wan, G., Liu, X., 2017. Mechanism and kinetics studies of carboxyl group formation on the surface of cellulose fiber in a TEMPO-mediated system. Cellulose 24 (6), 2415–2425. https://doi.org/10.1007/s10570-017-1279-9.
Sangian, H.F., Sehe, M.R., Tamuntuan, G.H., Zulnazri, Z., 2018. Utilization of saline solutions in the modification of lignocellulose from champaca wood. Journal of the Korean Wood Science and Technology 46 (4), 368–379. https://doi.org/10.5658/WOOD.2018.46.4.368.
Sayakulu, N.F., Soloi, S., 2022. The effect of sodium hydroxide (NaOH) concentration on oil palm empty fruit bunch (OPEFB) cellulose yield. J. Phys. Conf. 2314 (1), 1–8. https://doi.org/10.1088/1742-6596/2314/1/012017.
Schvartz, T., Shoseyov, O., 2022. Defibrillated microcrystalline cellulose as an efficient emulsion stabilizer – study of food-grade Pickering emulsions resistant to extreme conditions. Lebensm. Wiss. Technol. 155, 1–11. https://doi.org/10.1016/j.lwt.2021.113006.
Segal, L., Creely, J.J., Martin, A.E., Conrad, C.M., 1959. An empirical method for estimating the degree of crystallinity of native cellulose using the x-ray diffractometer. Textil. Res. J. 29 (10), 786–794. https://doi.org/10.1177/004051755902901003.
Seki, T., Chiang, K.Y., Yu, C.C., Yu, X., Okuno, M., Hunger, J., Nagata, Y., Bonn, M., 2020. The bending mode of water: a powerful probe for hydrogen bond structure of aqueous systems. J. Phys. Chem. Lett. 11 (19), 1–35. https://doi.org/10.1021/acs.jpclett.0c01259.
Sharma, P.R., Varma, A.J., 2014. Functionalized celluloses and their nanoparticles: morphology, thermal properties, and solubility studies. Carbohydr. Polym. 104 (1), 135–142. https://doi.org/10.1016/j.carbpol.2014.01.015.
Shen, Z., Rajabi-Abhari, A., Oh, K., Yang, G., Youn, H.J., Lee, H.L., 2021. Improving the barrier properties of packaging paper by polyvinyl alcohol based polymer coating—effect of the base paper and nanoclay. Polymers 13 (8), 1334. https://doi.org/10.3390/polym13081334.
Shi, S., Zhang, M., Ling, C., Hou, W., Yan, Z., 2018. Extraction and characterization of microcrystalline cellulose from waste cotton fabrics via hydrothermal method. Waste Manag. 82, 139–146. https://doi.org/10.1016/j.wasman.2018.10.023.
Silvia, S., Maharani, A., 2023. The effect of enzyme concentration and hydrolysis time on the yield of microcrystalline cellulose from rice straw. Dinasti Health and Pharmacy Science 1 (1), 25–32. https://doi.org/10.38035/dhps.v1i1.243.
Söz, Ç., 2022. Mechanical and wetting properties of coated paper sheets with varying polydimethylsiloxane molecular masses in the coating formulation. Turk. J. Chem. 46 (1), 283–294. https://doi.org/10.3906/kim-2104-57.
Sridhar, V., Park, H., 2020. Extraction of microfibrillar cellulose from waste paper by NaOH/urethane aqueous system and its utility in removal of lead from contaminated water. Materials 13 (12), 2850. https://doi.org/10.3390/ma13122850.
Sriprom, W., Sirivallop, A., Choodum, A., Limsakul, W., Wongniramaikul, W., 2022. Plastic/natural fiber composite based on recycled expanded polystyrene foam waste. Polymers 14 (11), 1–11. https://doi.org/10.3390/polym14112241.
Stojicic, S., Zivkovic, S., Qian, W., Zhang, H., Haapasalo, M., 2010. Tissue dissolution by sodium hypochlorite: effect of concentration, temperature, agitation, and surfactant. J. Endod. 36 (9), 1558–1562. https://doi.org/10.1016/j.joen.2010.06.021.
Stricker, M., Weygand, D., 2024. A model for physical dislocation transmission through grain boundaries and its implementation in a discrete dislocation dynamics tool. J. Mater. Sci.: Materials Theory 8 (1), 12. https://doi.org/10.1186/s41313-024-00065-7.
Syamani, F.A., Subyakto, Sukardi, Suryani, A., 2015. Changes in oil palm frond fiber morphology, cellulose crystallinity and chemical functional groups during cellulose extraction phases. Chem. Mater. Res. 7 (3), 113–121. www.iiste.org.
Trache, D., Tarchoun, A.F., Derradji, M., Hamidon, T.S., Masruchin, N., Brosse, N., Hussin, M.H., 2020. Nanocellulose: from fundamentals to advanced applications. Front. Chem. 8 (May), 1–33. https://doi.org/10.3389/fchem.2020.00392.
Trisant, P.N., Gunardi, I., Sumarno, 2020. The influence of hydrolysis time in hydrothermal process of cellulose from sengon wood sawdust. Macromol. Symp. 391 (1), 1–5. https://doi.org/10.1002/masy.202000016.
Trivedi, M.K., Mani, G.C.S., Pooniwala, N.K., 1979. Physical properties of base papers used in packaging. Indian Pulp & Paper Technical Association XVI (2), 94–97.
Unwaste trendspotting alert. (2023). In United Nations Office on Drugs and Crime.
Uyigue, L., Okwonna, O.O., 2013. Conversion of post-consumer (or waste) printers' paper grades into microcrystalline cellulose powder. J. Emerg. Trends Eng. Appl. Sci. 4 (1), 126–132.
Verma, D., Goh, K.L., 2021. Effect of mercerization/alkali surface treatment of natural fibres and their utilization in polymer composites: mechanical and morphological studies. Journal of Composites Science 5 (7). https://doi.org/10.3390/jcs5070175.
Vicente, A.T., Araújo, A., Gaspar, D., Santos, L., Marques, A.C., Mendes, M.J., Pereira, L., Fortunato, E., Martins, R., 2017. Optoelectronics and bio devices on paper powered by solar cells. Nanostructured Solar Cells 7688 (264687), 33–65. https://doi.org/10.5772/66695. InTech.
Vora, R.S., Shah, Y.D., 2015. Production of micro crystalline cellulose from corn husk and its evaluation as pharmaceutical excipient. International Journal of Research and Scientific Innovation 2 (11), 69–74. https://www.rsisinternational.org/Issue20/69-74.pdf.
Wahlström, N., Edlund, U., Pavia, H., Toth, G., Jaworski, A., Pell, A.J., Choong, F.X., Shirani, H., Nilsson, K.P.R., Richter-Dahlfors, A., 2020. Cellulose from the green macroalgae Ulva lactuca: isolation, characterization, optotracing, and production of cellulose nanofibrils. Cellulose 27 (7), 3707–3725. https://doi.org/10.1007/s10570-020-03029-5.
Wakeman, R., 2007. The influence of particle properties on filtration. Separ. Purif. Technol. 58 (2), 234–241. https://doi.org/10.1016/j.seppur.2007.03.018.
Wang, J., Minami, E., Asmadi, M., Kawamoto, H., 2021. Effect of delignification on thermal degradation reactivities of hemicellulose and cellulose in wood cell walls. J. Wood Sci. 67 (1), 19. https://doi.org/10.1186/s10086-021-01952-0.
Wang, R., Zhou, B., Wang, Z., 2019. Study on the preparation and application of lignin-derived polycarboxylic acids. J. Chem. 2019, 1–8. https://doi.org/10.1155/2019/5493745.
Wang, T., Zhao, Y., 2021. Optimization of bleaching process for cellulose extraction from apple and kale pomace and evaluation of their potentials as film forming materials. Carbohydr. Polym. 253 (August 2020), 1–11. https://doi.org/10.1016/j.carbpol.2020.117225.
Wei, Y., Li, Z., 2016. Measurement of d-spacing of crystalline samples with SAXS. Measurement 93, 473–479. https://doi.org/10.1016/j.measurement.2016.07.051.

Wu, J., Ding, Q., Yang, W., Wang, L., Wang, H., 2021. Influence of submicron fibrillated cellulose fibers from cotton on hydration and microstructure of portland cement paste. Molecules 26 (19), 1–13. https://doi.org/10.3390/molecules26195831.

Xiang, X., Liu, N., Xu, L., Cai, Y., 2021. Review of recent findings on occurrence and fates of siloxanes in environmental compartments. Ecotoxicol. Environ. Saf. 224, 112631. https://doi.org/10.1016/j.ecoenv.2021.112631.

Xiu, H., Cheng, R., Li, J., Ma, F., Song, T., Yang, X., Feng, P., Zhang, X., Kozliak, E., Ji, Y., 2019. Effects of acid hydrolysis waste liquid recycle on preparation of microcrystalline cellulose. Green Process. Synth. 8 (1), 348–354. https://doi.org/10.1515/gps-2019-0002.

Yang, J., Wang, X., Shen, F., Qi, X., 2021. Base activation of persulfate: an effective pretreatment method to enhance glucose production from lignocellulosic biomass. Cellulose 28 (7), 4039–4051. https://doi.org/10.1007/s10570-021-03796-9.

Zaki, S.N.R.M., Buniyamin, I., Mahmood, M.R., Zakaria, M.N., 2022. Characterization of microcrystalline cellulose isolated from paper sludge. International Conference on Wood and Eco-Products 2022 455–460.

Žgajnar Gotvajn, A., Kalčíková, G., 2018. Delamination of plastic-coated waste paper by enzymes of the white rot fungus Dichomitus squalens. J. Environ. Manag. 228 (January), 165–168. https://doi.org/10.1016/j.jenvman.2018.08.111.

Zhang, J., Huo, H., Zhang, L., Yang, Y., Li, H., Ren, Y., Zhang, Z., 2022. Effect of high-temperature hydrothermal treatment on the cellulose derived from the buxus plant. Polymers 14 (10), 1–11. https://doi.org/10.3390/polym14102053.

Zhao, H., Zhao, L., Lin, X., Shen, L., 2022. An update on microcrystalline cellulose in direct compression: functionality, critical material attributes, and co-processed excipients. Carbohydr. Polym. 278 (December 2021), 1–15. https://doi.org/10.1016/j.carbpol.2021.118968.

Zhou, X., Li, X.Y., Lu, K., 2018. Enhanced thermal stability of nanograined metals below a critical grain size. Science 360 (6388), 526–530. https://doi.org/10.1126/science.aar6941.

Zhu, C., Krumm, C., Facas, G.G., Neurock, M., Dauenhauer, P.J., 2017. Energetics of cellulose and cyclodextrin glycosidic bond cleavage. React. Chem. Eng. https://doi.org/10.1039/C6RE00176A. September 2019.

Zielecka, M., Rabajczyk, A., Pastuszka, Ł., Jurecki, L., 2020. Flame resistant silicone-containing coating materials. Coatings 10 (5), 479. https://doi.org/10.3390/coatings10050479.

Paswan, S.K., Kumari, S., Kar, M., Singh, A., Pathak, H., Borah, J.P., Kumar, L., 2021. Optimization of structure-property relationships in nickel ferrite nanoparticles annealed at different temperature. J. Phys. Chem. Solid. 151 (December 2020), 1–26. doi:10.1016/j.jpcs.2020.109928.